Phased Antenna Array for 26-40 GHz Band

Henri Kähkönen

School of Electrical Engineering

Thesis submitted for examination for the degree of Master of Science in Technology.

Espoo 22.5.2017

Thesis supervisor:

Prof. Ville Viikari

Thesis advisor:

D.Sc. (Tech.) Juha Ala-Laurinaho

Aalto University
School of Electrical
Engineering

AALTO UNIVERSITY
SCHOOL OF ELECTRICAL ENGINEERING

ABSTRACT OF THE
MASTER'S THESIS

Author: Henri Kähkönen

Title: Phased Antenna Array for 26-40 GHz Band

Date: 22.5.2017 Language: English Number of pages: 8+58

Department of Electronics and Nanoengineering

Supervisor: Prof. Ville Viikari

Advisor: D.Sc. (Tech.) Juha Ala-Laurinaho

This thesis studies what kind of antenna elements could be used in phased arrays at Ka-band (26–40 GHz). The arrays studied should have efficiency above 90% at the whole Ka-band and when steered up to 60° away from the boresight. Additionally, the element pattern should be free of any scan blindness.

Aperture coupled stacked microstrip patch element and two different flared-notch elements are studied by performing electromagnetic simulations. The simulations are first conducted in an infinite array environment with periodic boundary conditions. After these three elements are simulated and optimized, the element which has the best performance while still being manufacturable is chosen for simulations in finite 8×8 array.

The flared-notch element which was selected for further simulation fulfills almost all of the requirements except that for the efficiency. However, it exhibits 90% efficiency throughout most of the required frequency band and steering angles without any scan blindness. The active element pattern has the half power beamwidth of 120° which allows for ±60° steering range with scan loss of 3 dB at maximum. The simulation results in finite array configuration are well in line with the previous simulations in the infinite array.

Keywords: phased array, array antenna, Ka-band, tapered slot antenna, flared-notch antenna, Vivaldi antenna, wide-band antennas, stacked patch antenna

AALTO-YLIOPISTO
SÄHKÖTEKNIIKAN KORKEAKOULU

DIPLOMITYÖN
TIIVISTELMÄ

Tekijä: Henri Kähkönen

Työn nimi: Vaiheistettu antenniryhmä 26–40 GHz:n kaistalle

Päivämäärä: 22.5.2017 Kieli: Englanti Sivumäärä: 8+58

Elektroniikan ja nanotekniikan laitos

Työn valvoja: Prof. Ville Viikari

Työn ohjaaja: TkT Juha Ala-Laurinaho

Tämän diplomityön tarkoituksena oli tutkia millaisia antenni elementtejä voitaisiin käyttää Ka-kaistan (26–40 GHz) vaiheohjatuissa antenniryhmissä. Työn aikana oli myös tavoitteena suunnitella edellä mainitulle kaistalle antennielementti, jonka hyötysuhde on vähintään 90% koko taajuuskaistalla myös silloin kun antenniryhmän pääkeilaa ohjataan 0°–60° kohtisuoraan säteilyyn verrattuna. Lisäksi antennin aktiivisen suuntakuvion keilanleveyden tulisi olla 120°.

Rako kytkettyä kerrostettua mikroliuska-antennielementtiä ja kahta erilaista Vivaldi antenni elementtiä tutkitaan sähkömagneettisien simulaatioiden avulla. Aluksi simulaatiot toteutetaan äärettömässä antenniryhmässä jaksollisen reunaehdon avulla. Kun kolmen edellämainitun antennirakenteen parametrit on optimoitu valitaan simulaatiotulosten ja rakenteiden valmistettavuuden perusteella lupaavin rakenne, joka simuloidaan äärellisessä 8×8 antenniryhmässä.

Vivaldi elementti joka valittiin lupaavimmaksi rakenteeksi toimii simulaatioiden perusteella lähes koko taajuuskaistalla yli 90% hyötysuhteella ottamatta huomioon joitakin keilan kääntökulmia suurilla taajuuksilla. Antennin aktiivisen suuntakuvion keilanleveys on 120°. Simulaatiotulokset äärellisessä antenniryhmässä vastaavat hyvin simulaatiotuloksia äärettömässä antenniryhmässä.

Avainsanat: antenniryhmä, vaiheistettu antenniryhmä, laajakaista–antennit, Vivaldi–antenni, mikroliuska–antenni, Ka-kaista

Preface

This thesis has been the final push towards completing my M.Sc. (Tech.) degree and I would like to thank those without whom this thesis would not have been possible. First, I would like to thank Prof. Ville Viikari for supervising my thesis and above all giving me an opportunity to work on this interesting subject. I would also like to thank D.Sc. (Tech.) Juha Ala-Laurinaho for all the advises, comments, and discussions regarding this thesis. This project was a part of the new collaboration between Aalto university and Saab Ab and I would like to express my gratitude to Saab for funding this project.

Even though the studies in Otaniemi have been only one small part of my life I would also like to thank all the friends and colleagues I have made during my studies. Finally, I would like to thank my family for all the support I have received.

Otaniemi, 22.05.2017

Henri Kähkönen

Contents

Symbols and abbreviations

Symbols

A_{array}	area of an array
A_{cell}	area of an aperture
A_n	amplitude tuning term of branch n
AF	array factor
c	speed of light in vacuum $\approx 3 \times 10^8$ [m/s]
D	directivity
$D_{MaxArray}$	maximum directivity of an array
$D_{MaxCell}$	maximum directivity of an aperture
d	distance between antenna elements in an array
e_c	conduction efficiency
e_{cd}	radiation efficiency
e_d	dielectric efficiency
e_r	reflection efficiency
e_0	total efficiency
$F(\theta, \phi)$	total approx. radiated power at direction (θ, ϕ)
f	frequency
$f(\theta, \phi)$	array factor at direction (θ, ϕ)
G	gain
G^R	realized gain
$G_a(\theta, \phi)$	gain of an array at direction (θ, ϕ)
$G_{ae}(\theta, \phi)$	active element pattern at direction (θ, ϕ)
$G_0(\theta, \phi)$	gain of an isolated antenna at direction (θ, ϕ)
I	current
I_n	phase and amplitude tuning term of branch n
P_{in}	total accepted power
P_{rad}	total radiated power
R_A	antenna resistance
S_{ij}	scattering parameter to port i from port j
$\tan \delta$	dissipation factor
U	radiation intensity
U_0	radiation intensity of an isotropic antenna
V	voltage
x	Cartesian x-coordinate
X_A	antenna reactance
y	Cartesian y-coordinate
Z	impedance
z	Cartesian z-coordinate
Z_A	antenna impedance
Z_{nn}	self-impedance of nth element
Z_{nm}	mutual impedance between nth and mth element
Z_0	characteristic impedance

α	beam steering angle
α_{mn}	phase term
β	wave constant $= 2\pi/\lambda$
Γ	reflection coefficient
$\Gamma(\theta, \phi)$	reflection coefficient at direction (θ, ϕ)
ϵ	permittivity
ϵ_L	aperture efficiency
ϵ_r	relative permittivity
ϵ_0	vacuum permittivity $\approx 8.8541878176 \times 10^{-12}$ F/m
θ	beam steering angle in spherical coordinates
θ_0	direction of the main lobe
θ_{GL}	direction of the grating lobe
λ	wavelength
μ	permeability
μ_0	vacuum permeability $= 4\pi \times 10^{-7}\ N/A^2$
ξ_n	relative phase of signal of nth element
π	mathematical constant = 3.141592653...
ϕ	beam steering angle in spherical coordinates
ϕ_0	direction of main lobe

Abbreviations

A/D	Analog-to-digital
AEI	Active element impedance
AEP	Active element pattern
ARC	Active reflection coefficient
D/A	Digital-to-analog
EDM	Electric discharge machining
EM	Electromagnetic
EW	Electronic warfare
HPBW	Half power beamwidth
IC	Integrated circuit
PCB	Printed circuit board
QTEM	Quasi tranverse electromagnetic
RF	Radio frequency
SLL	Sidelobe level
TEM	Transverse electromagnetic
VNA	Vector network analyzer

1 Introduction

Phased arrays were first used during second world war in radars. Today phased arrays are most commonly used in different types of radars but can also be used in communication and acoustics. Radar is an electromagnetic system for detecting reflective object and it operates by sending energy into space and detecting the echoes created by the environment. Radar can be used for example for military purposes, remote sensing, air traffic control, navigation, and safety systems in cars. For military purposes or electronic warfare (EW), active or passive radars (radiometers) are used. Active radar send energy and detect the echo and passive radars can be used to detect enemy's electromagnetic emissions without emitting any additional energy. [1], [2]

The accuracy of a radar can generally be separated in two parts, the angular accuracy and the range resolution. Angular accuracy is strongly related to the beamwidth of the antenna pattern and the range accuracy in pulse radars depends on the pulse length or in intrapulse-modulation radar on the bandwidth of the signal. Both the beamwidth and the bandwidth of the system have a relation to the frequency and both can be increased by increasing the frequency. As the beamwidth of an antenna is strongly related to the ratio between the frequency and the area of the radiator the beamwidth becomes narrower if the antenna size is not changed. As the frequency increases and the relative bandwidth is not changed the absolute bandwidth increases thus increasing the range accuracy. [1]

From the steering point of view, radars can be divided in to two groups: mechanically steered and electrically steered. Mechanically steered antennas as the name suggest, rely on mechanical steering where usually a single antenna is steered. Mechanically steered antennas are usually quite simple to construct but they require often heavy and large support structures and motors. On the other hand, as there is only one antenna the frequency can be increased with little effort. Electrically steered antennas or phased arrays are constructed from multiple small antenna elements and are steered by controlling the signals fed into each element. In phased arrays, the antenna can be made lighter and conformed to, e.g., a hull of vehicle, but the feeding network can be quite complex. Additionally, the antennas in phased array have to be completely redesigned when a higher frequency system is desired. [1], [3]

A lot of research on phased arrays has been done for frequencies below Ka-band. However, very little research on phased array antennas with bandwidth that could cover the whole Ka-band with 60° beam steering have been carried out. The purpose of this thesis is to study possible wide-band antenna array elements for Ka-band for future applications and it is carried out in collaboration with Saab [4].In this thesis, suitable wide-band antenna elements for phased array applications are studied based on previous research found from literature and then, an antenna array element in an infinite array is design according to defined specifications and simulation results of the designed structures are presented. Finally, the most suitable structure is simulated in 8×8 array. The 8×8 array will be manufactured during a following project, in which the simulation results and the measurement results from the manufactured array will be compared. The phased array antenna designed here should operate throughout the whole Ka-band from 26 GHz to 40 GHz, to be steerable up to 60°

in any direction from boresight, and to support two orthogonal linear polarizations. The efficiency of the designed antenna covering the aforementioned frequency range and beam steering should also stay above 90% at all steering angles throughout the frequency range. Each antenna element in the array should also be designed so that the element spacing in the array is maximum of $\lambda/2$ to prevent any grating lobes emerging when the antenna beam is steered. The challenge of designing phased arrays for frequencies as high as Ka-band and above is that the antenna element size at these frequencies is already quite small which can make the manufacturing of the antenna structure difficult.

This thesis is constructed from the following sections. In section 2, antenna properties and wide-band antennas are discussed. The most promising structures, stacked patch and flared-notch antennas, are discussed in more depth. The theory behind phased array antennas is discussed in section 3. In section 4, the design parameters of the stacked patch and flared-notch antenna structures for Ka-band are studied and the performance of each structure is presented. The flared-notch design is further divided in two different designs. The 8×8-element, manufacturable measurement prototype, simulation results, and possible measurement methods of the chosen structure are described in section 5. Finally, the thesis is concluded in section 6.

2 Antennas

An antenna is that part of a transmitting or receiving system that is designed to radiate or to receive electromagnetic waves [5]. The most interesting parameters to characterize antenna performance are impedance, bandwidth, polarization, directivity, gain, and radiation pattern. These will be explained in more detail in section 2.1.

Antennas can be classified for example under electrically small antennas, resonant antennas, broadband antennas, and aperture antennas. The broadband antennas are the most interesting type of antennas in the context of this thesis and they will be discussed in section 2.2.

When antennas are measured or simulated, some of the results should be presented so that the orientation of the antenna in relation to the results will be understood. It is important to define the orientation of the antenna with respect to the coordinate system [6]. Figure 1 shows the standard spherical coordinate system used in antenna measurements. In the results presented in this thesis, the antenna is positioned on the xy-plane in the origin such that the broadside is directed to $\theta = 0°$. For x-polarized antenna the planes where ϕ is 0°, 45°, and 90° are referred as E-, D-, and H-planes.

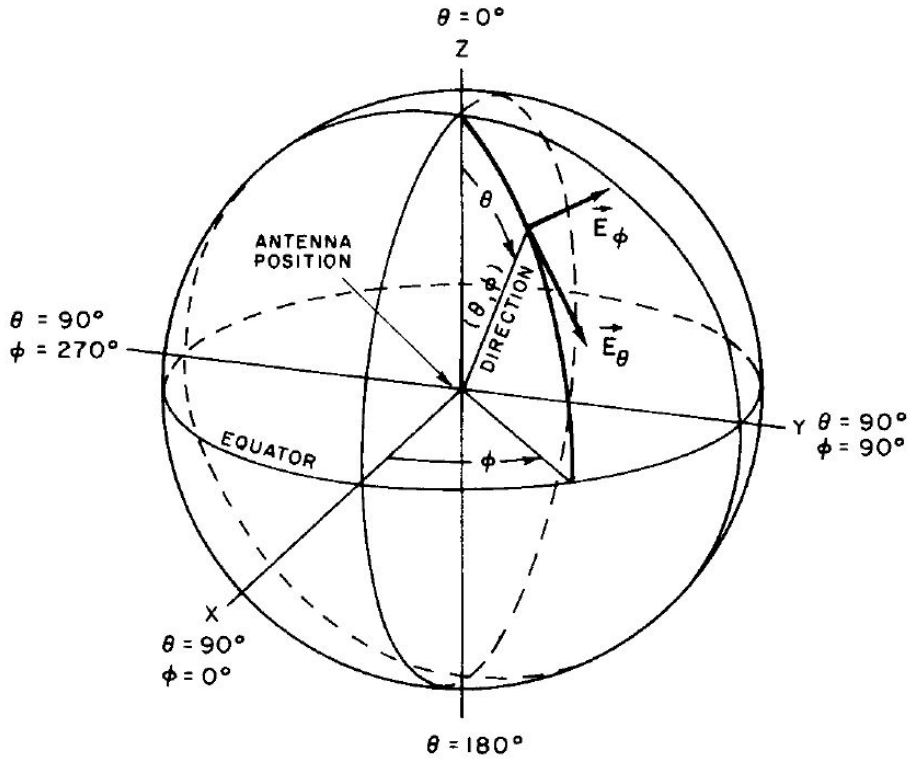

Figure 1: Standard spherical coordinate system used in antenna measurements. [6]

2.1 Antenna properties

Fundamental antenna properties are impedance, bandwidth, polarization, efficiency, directivity, gain, and radiation pattern. These are the major properties of antennas which have to be considered when an antenna is chosen for a specific application. Each of these properties are explained here in more detail.

2.1.1 Impedance

The impedance of the antenna depends on the antenna structure and the environment [7]. For example, other antennas in the vicinity of the observed antenna will have an effect on the observed antenna. This phenomenon is known as mutual coupling and it is very apparent in antenna arrays and will be more closely discussed later.

The antenna impedance is composed of real and imaginary parts as in regular circuits, and it is expressed as

$$Z_{\mathrm{A}} = R_{\mathrm{A}} + jX_{\mathrm{A}} \tag{1}$$

where R_A is the antenna resistance and X_A is the antenna reactance. The antenna resistance represents the power dissipated in the antenna and is composed of the radiation resistance and the resistance associated with losses occurring in the antenna structure. In electrically small antennas, the losses occurring in the antenna can be significant but in other antennas the losses are usually small compared to the radiated power. The reactance describes the energy stored in the near-field of the antenna. [7]

The impedance of the antenna and the transmitter or the receiver should be equal to minimize reflections and allow for maximum signal transfer. In reception, to match the receiver and antenna impedances, the receiver should be conjugate matched to the antenna. The conjugate matching means that the real parts of the impedance are equal and the reactance magnitudes are equal but have opposite sign. The impedance of the receivers is resistive, usually $50\,\Omega$, thus it is required to use matching network in between the receiver and the antenna. Disadvantages of the matching network are the ohmic losses and the matching is usually achieved only over narrow frequency band. [7]

2.1.2 Efficiency

The total efficiency of the antenna can be expressed as

$$e_0 = e_{\mathrm{r}} e_{\mathrm{cd}} \tag{2}$$

where e_{r} is the reflection efficiency $(1-|\Gamma|^2)$ and e_{cd} is the radiation efficiency which includes the dielectric and conduction efficiency [8]. Dielectric and conduction efficiencies take into account the energy lost due to the losses in the dielectric and metals in the antenna element. The total efficiency is strongly related to the reflection coefficient of the antenna. In case of electrically small antennas, where the radiation efficiency can be low, the efficiency is usually more useful figure of merit than the reflection coefficient as the efficiency also includes the radiation losses.

2.1.3 Bandwidth

The bandwidth describes the continuous desired operation frequency range where the important antenna performance parameters are acceptable. The bandwidth is usually presented as a ratio between the upper and lower frequencies or as a percentage with respect to the center frequency. [7]

Usually, the bandwidth of an antenna is defined from the measured or simulated reflection coefficient from the antenna input port or from a port which includes an antenna and a matching circuit. For example, a level of acceptable reflection coefficient is defined and the frequency band at which the reflection coefficient is measured to be lower is the antenna bandwidth. Reflection coefficient alone is not always the most suitable parameter to be used to define the bandwidth especially when a matching network is required as there might be significant ohmic losses. Other popular parameters to define the bandwidth are for example the antenna efficiency and the gain. [8]

2.1.4 Polarization

When observed far enough, the wave front radiated by an antenna can generally be defined as a plane wave and the electric and magnetic field vectors are on this plane. The polarization of a plane wave describes the electric field vector behave as a function of time at a fixed point and it can always be expressed as a combination of two linear components, i.e. x- and y-polarizations. Polarization can be either linear, circular, or elliptical. If the electric field vector is always directed along the same line, the polarization is linear. Generally, the polarization of the field is always elliptical polarization, whereas linear and circular polarizations are just a special cases of elliptical polarization. Elliptical polarization can be either right- or left-hand polarized depending on the direction of the field vector rotation. When the field is observed along the propagation direction clockwise rotation corresponds to right-hand polarization and counterclockwise rotation corresponds to left-hand polarization. [7]

Linear polarization is achieved only when the time-phase difference between the two orthogonal components is a multiple of π or the magnitude of the other component is zero. Circular polarization is achieved only when the time-phase difference between the two orthogonal linear components is an odd multiple of $\pi/2$ and the magnitude of the components is equal. Elliptical polarization is achieved when the time-phase difference of the two components is an odd multiple of $\pi/2$ and the magnitudes of the components are not equal or when the time-phase difference is not equal to a multiple of $\pi/2$. [8]

2.1.5 Directivity and gain

The directivity of an antenna is the ratio ratio of the radiation intensity to a given direction compared to a radiation intensity of an isotropic radiator [7]. Mathematically it can be expressed as

$$D = \frac{U}{U_0} = \frac{4\pi U}{P_{\text{rad}}} \tag{3}$$

where D is the directivity, U is the radiation intensity, U_0 is the radiation intensity of an isotropic radiator, and P_{rad} is the total radiated power [8]. Usually, U is the intensity to the direction where the radiation intensity is strongest but it can be calculated to any angle.

The directivity takes into account only the directional properties of an antenna. A property more closely related to measurements is the gain. In addition to the directional properties of an antenna, the gain takes also into account the radiation efficiency. When the directivity is a ratio between the radiation intensity and the radiated power, the gain is a ratio between the radiation intensity and the total accepted power and can be written as

$$G = \frac{4\pi U}{P_{\text{in}}} = e_{\text{cd}} \frac{4\pi U}{P_{\text{rad}}} \tag{4}$$

where P_{in} is the total accepted power [8].

2.1.6 Radiation pattern

In [5], radiation pattern is defined as "The spatial distribution of a quantity that characterizes the electromagnetic field generated by an antenna." The coordinate system shown in Figure 1 is used to present the pattern either in three dimensional form or as a planar cut as a function of θ and ϕ. The pattern can be presented either as a field pattern which represents the electric or magnetic field magnitude as a function of angular space, or as a power pattern which is square of the field pattern. [8] Usually radiation patterns are presented as normalized patterns in such a way that the maximum value equals unity [7]. The most convenient presentation form of the field and the power patterns is the logarithmic scale because in directive antennas the differences between high and low values can be quite large.

2.2 Broadband antennas

The most interesting antennas regarding this thesis are antennas that have relatively large bandwidth and are thus called broadband antennas. Broadband antenna is defined in [5] as "An antenna the bandwidth of which is of the order of or greater than 2:1." Broadband antennas are usually constructed with smooth curves and geometries and do not have abrupt changes in dimensions [7]. Smooth geometries produce frequency response that is generally smooth which is essential for broadband operation. Some well known broadband antennas are log-periodic antennas, spiral antennas, biconical antennas, and traveling-wave antennas [7]. Resonant antennas

rarely qualify as broadband as the structures of these antennas are usually related to the wavelength of the signal.

Broadband antennas have been studied since 1950s in an attempt to increase the bandwidth of antennas [9], [10]. The first broadband antennas were generally exponential structures, for example exponentially increasing spiral or exponentially increasing slot [9], [11]. The general relation between broadband operation and logarithmically periodic structures was studied in depth in [10] and it has been used as a base for further studies. More recently, as the number of small consumer mobile devices has increased, even smaller broadband antenna structures have been studied [12], [13].

Broadband antennas that can be implemented in phased arrays are the most interesting in the scope of this thesis. A stacked patch antenna, where the bandwidth is increased with multiple resonant structures for different frequencies and the flared-notch antenna which is an exponentially increasing slot, are promising structures that can be used in phased arrays. These structures are discussed in more detail in the following sections.

2.2.1 Stacked patch antenna

Microstrip patch antennas are attractive antennas due to their easy manufacturing as they can be manufactured similarly as PCBs and used as the single radiating element in arrays. On the downside, regular patch antennas are resonant structures which are narrowband elements and the bandwidth is usually only a few percent of the operation frequency. The most simple microstrip patch antenna is a microstrip line fed square patch on top of a substrate and a ground plane. When the side of the square patch is d, the antenna resonates approximately at a frequency at which d equals $\lambda/2$ [7]. The bandwidth of a regular microstrip antenna can be slightly increased with an aperture coupled microstrip feed in which the aperture acts as the second resonator [14].

The bandwidth of patch antennas can be further increased by adding another parasitic patch on top of the primary patch as shown in Figure 2 [15]. A simple single polarized stacked patch structure is generally constructed from three layers. The first layer includes the microstrip at the bottom of the substrate and the ground plane and aperture in the ground plane above the substrate. The second layer is the primary patch and its substrate, and the third layer is the parasitic microstrip patch and its substrate. In addition to the aperture coupled microstrip, another popular feed structure for stacked patches is electromagnetic coupling, for example a coaxial cable which has galvanic connections to the first patch and the ground plane. The increased bandwidth in stacked patches is caused by effect of the two patches which resonate at near frequencies and yields broadband effect [7]. Usually the parasitic upper patch is electrically slightly smaller than the lower patch an thus it resonates at higher frequency. The resonance effect of these two patches can be increased by increasing the spacing between them. This is usually done by incorporating an air gap or gap filled with low dielectric constant foam. In this kind of structure where the patches are on thick substrates, they act as low-Q resonators increasing the

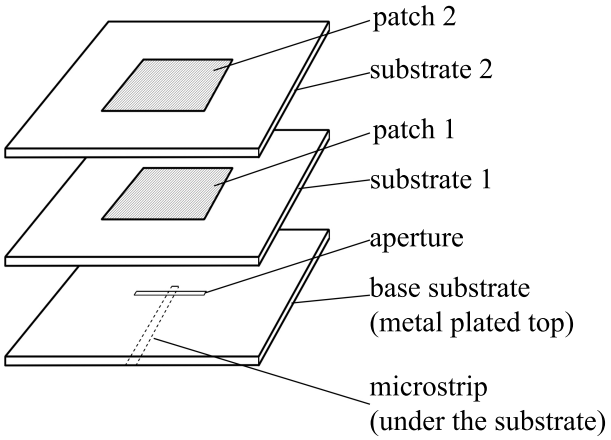

Figure 2: A general stacked patch antenna which is fed with aperture coupled microstrip.

bandwidth even further. When the stacked patches are combined with the aperture coupled feed which acts as the second resonator the bandwidth can be increase even up to 70 % [16]. The downside of the thick substrates is that in phased arrays the thicker substrates increases the generation of surface waves which are the main cause for high cross-polarization and scan blindness in beam-steering phased arrays [7].

The stacked patch antenna can also be realized in dual-polarized configuration. The electromagnetically coupled (galvanic connection) feed would be the easiest to implement as it is basically only a vertical probe brought through the ground plane and connected galvanically under the patch. The wider bandwidth aperture coupled feed is considerably harder to implement as the aperture takes more space and usually situated in the middle under the patch. In [17] is presented one option to implement dual-polarized aperture feed. The feeds are realized by splitting each feed microstrip in two with a reactive power combiner and then feed a centrally located cross-shaped slot. The microstrips of the different polarizations are routed on perpendicular sides of the slot plane.

2.2.2 Flared-notch antenna

Flared-notch or Vivaldi antenna was first presented in 1979 in [11] and since then it has been used in multiple of studies in single and array antenna configurations [18–21]. It is well known for its potential for ultra wide frequency band and has characteristics that are well suited for array applications. The radiation from a Vivaldi antenna is linearly polarized and the radiation pattern is close to symmetrical on E- and H-planes and stable with frequency making it a major candidate when designing a wide band phased array in which the array does not need to be of the most low-profile.

A general flared-notch antenna geometry is shown in Figure 3. The antenna is constructed from a metal fin in free space or on top of a dielectric. The antenna design is carved to the fin and it includes the slot line the width of which increases towards the radiating end of the antenna and a cavity connected to the narrow end of the slot line as seen in the figure. The flare is used to match the impedance of the

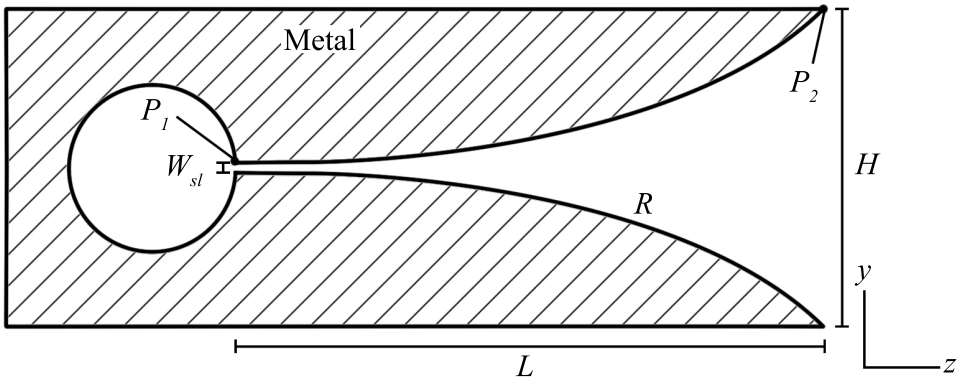

Figure 3: A general shape of a flared-notch antenna.

feed to the free space wave impedance (377 Ω). The antenna element can be fed with a few different options. For example, a coaxial line connected straight across the slot line close the cavity or a microstrip line which is routed across the slot line on the other side of a substrate and utilizes the metal fin as a ground plane. The size of the cavity modifies the antenna resistance and reactance, and it can be used to optimize the matching of the antenna to suite the feed method of the antenna [18]. The shape of the cavity is not restricted to a circle and it can also be a square or a rectangle but the overall length of the cavity from the feed point is usually $\lambda/4$ to increase forward gain and matching [21]. For the best matching the width of the slot line W_{sl} should be set so that the impedance of the feed line and the slot line are identical. For example, if the antenna is fed with a 50-Ω coaxial cable the impedance of the slot line should also be 50 Ω. The length L and the opening rate R of the exponential taper, and the height of the aperture H are different if the element is used as a single antenna or if it is used as a part of an array [20]. The exponential tapering can be expressed as a function of the length of the taper, the rate of tapering and the height of the element with the start point $P_1(z_1, y_1)$ and the end point $P_2(z_2, y_2)$ of the flare as

$$y = c_1 e^{Rz} + c_2 \tag{5}$$

where

$$c_1 = \frac{y_2 - y_1}{e^{Rz_2} - e^{Rz_1}}, \tag{6}$$

$$c_2 = \frac{y_1 e^{Rz_2} - y_2 e^{Rz_1}}{e^{Rz_2} - e^{Rz_1}}, \quad \text{and} \tag{7}$$

where R is a positive opening rate usually between 0 and 1. When R=0 the tapering between P_1 and P_2 is linear [18].

The optimal operation of a single Vivaldi antenna is that of a traveling wave antenna. This kind of an antenna is usually frequency independent and the usable bandwidth is wide, even up to 6:1 [11]. The gain of the antenna is throughout the operation range approximately 10 dBi. To support the traveling wave mode, the width of the aperture should be larger than $\lambda/2$ and the length of the antenna at least one wavelength [20].

When a Vivaldi element is used in an array the best performance is achieved when the mutual coupling is used correctly. As the element spacing in phased arrays should be no more than $\lambda/2$ at the highest operation frequency, the Vivaldi antenna is too small to operate in traveling wave mode [20]. By properly using the mutual coupling to match the Vivaldi element in an array, bandwidths of even 8:1 can be achieved for 45° scan angles.

3 Array antennas

An array antenna may be composed of two to thousands of single antenna elements usually in linear or planar configuration and usually each element is fed coherently. Arrays can be used for example in place of large reflector antennas and the main benefit of arrays compared to other large aperture antennas is the capability for electronic beam steering. A conventional single aperture antenna requires mechanical components to steer the beam which restricts the speed of the steering and are usually bulky. Array antenna, or in this case phased array, is restricted only by the speed of the electronics behind the antenna as the beam of the array is controlled by changing the phase of the signal fed to each antenna. The phase of the signal can be changed for example with phase shifters, true time delay lines or directly in the signal generation if each element has its own transmitter or receiver . Populating each element in the array with its own electronics has become more feasible as the electronics have become faster, smaller and at the same time affordable. [7] [3]

In addition to being faster, the electronic steering allows more precise control of the beam. Depending on the electronics hardware, the beam can also be split into multiple beams and each can be steered separately. As the array is comprised of small elements, it is also possible to conform the shape of the array for example to the fuselage of an aircraft which increases the possibilities to implement various large sensors and radars without huge unwanted protrusions. [3]

The main properties that should be considered when designing an array antenna are array factor, grating lobes, gain, active element impedance, and active element pattern which will be discussed in-depth in the following subsections. Only linear or planar arrays will be considered in the explanation of the previously mentioned properties during this thesis.

3.1 Array factor

The array factor is a fundamental concept when array antennas are discussed and can itself be used to observe some of the important properties of an array without the characteristics of antenna elements.The array factor describes the radiation pattern of an array of isotropic elements. It is identical in both transmitting and receiving operations and in most cases also antennas are reciprocal components. The array factor can be manipulated by changing the phase and the amplitude of each element. [7]

The array factor for a linear array shown in Figure 4 is found by replacing the radiating elements in the array with isotropic radiators. The wavefront chosen as the reference is traveling to the direction arrives to the array in an angle θ and excites each element at the same power due to the characteristics of the plane wave. One element is chosen as the reference where the phase of the wavefront is set to zero. The other elements receive the same wavefront at some phase difference due to the different path length corresponding to the distance between the element and the reference element and the angle θ. The relative phase of the signal is ξ_i, when $i = 0$, 1, ..., n. In phased arrays, each antenna element can have a separate phase shifter

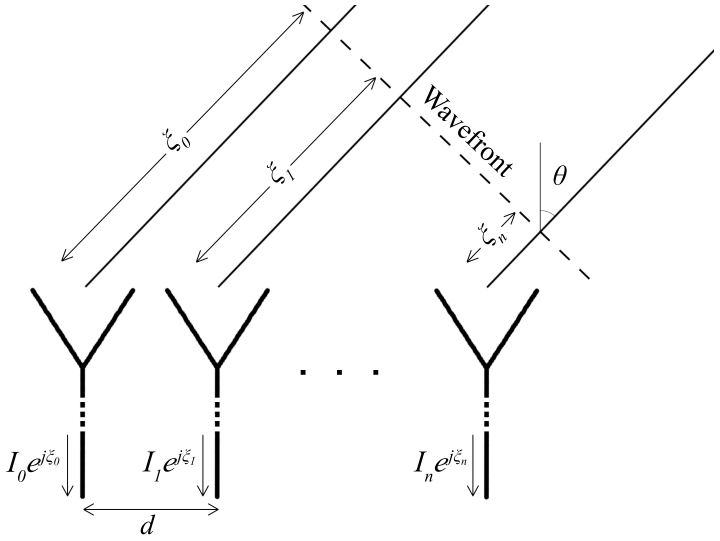

Figure 4: Illustration of a linear array for calculating the array factor.

and amplitude tuner. Signals from each antenna branch are combined and as a result the array factor can be expressed as

$$\begin{aligned} AF &= I_0 e^{j\xi_0} + I_1 e^{j\xi_1} + I_2 e^{j\xi_2} + \dots \\ &= I_0 + I_1 e^{j\beta d sin\theta} + I_2 e^{j\beta 2 d sin\theta} + \dots \\ &= \sum_{n=0}^{N-1} I_n e^{j\beta n d sin\theta} \end{aligned} \tag{8}$$

where each antenna branch contains a phase and amplitude tuning term I_n. It contains variable for amplitude (A_n) and phase (α) and can be expressed as

$$I_n = A_n e^{jn\alpha}. \tag{9}$$

Finally, when equations (8) and (9) are combined the array factor can be expressed as

$$AF = \sum_{n=0}^{N-1} A_n e^{jn(\beta d sin\theta + \alpha)} \tag{10}$$

where n is the number of the element (0 = reference element with zero phase shift), β is the wave constant ($2\pi/\lambda$), d is the distance between two elements, θ is the angle at which the array factor is calculated, and α is the difference in phase of the signal fed to each branch and is directly related to the steering angle (0° = broadside radiation) [7].

Using the final equation (10), the array factor can be illustrated for a specific range. For example, Figure 5 presents the array factor for linear eight element array when the array factor is steered to 0°, 25°, and 50° with element spacing of $\lambda/2$. The array factor is plotted for values between $\theta = -90°$ and $\theta = 90°$. These values of θ correspond to the half space which is the most interesting range when later during the thesis infinite or large arrays with directive elements are discussed.

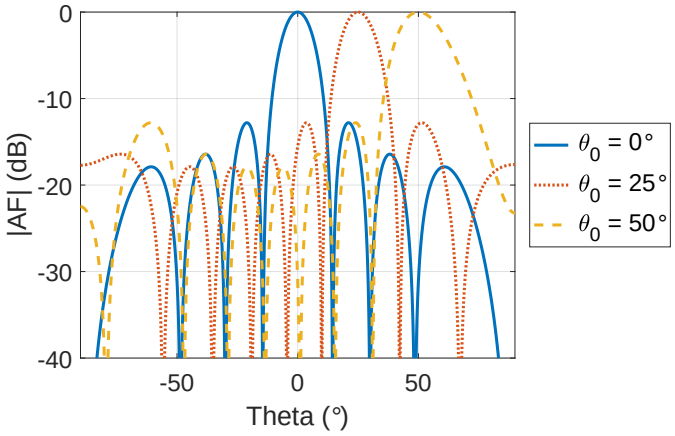

Figure 5: Normalized array factor of linear eight element array at different steering angles with element spacing of $\lambda/2$.

A linear array is quite restricted as it can scan only in one direction and the radiation pattern on the plane perpendicular to the array is as wide as the pattern of single element. Thus a number of applications require a planar or multidimensional array which can have narrow pencil beams and can be steered in all directions. Multidimensional array can have any shape, the array can be formed to follow a surface, and the elements in the array grid can have equal or unequal spacing.

The array factor calculation for a planar array follows the same principle as for the linear array. The elements are summed together with corresponding position vectors. For example, the position vector for an element in a planar array is

$$r'_{mn} = x'_{mn}\hat{\mathbf{x}} + y'_{mn}\hat{\mathbf{y}} \tag{11}$$

which replaces the term including the distance from the first element in the array factor for linear array. The array factor for a planar array which is the most interesting in the context of this thesis can then be derived from the generalized multidimensional array factor

$$AF = \sum_{n=1}^{N}\sum_{m=1}^{M} I_{mn} e^{j(\beta \hat{\mathbf{r}}\cdot\mathbf{r'_{mn}} + \alpha_{mn})} \tag{12}$$

where the term $\hat{\mathbf{r}} \cdot \mathbf{r'_{mn}}$ contains observation direction and the position vector as a function of θ and ϕ, and the phase term α_{mn} which contains position vectors and the man beam steering angles [7]. The resulting array factor for planar array is then

$$AF = \sum_{n=1}^{N}\sum_{m=1}^{M} I_{mn} e^{j\beta((x'_{mn}sin(\theta)cos(\phi)+y'_{mn}sin(\theta)sin(\phi))-(x'_{mn}sin(\theta_0)cos(\phi_0)+y'_{mn}sin(\theta_0)sin(\phi_0)))} \tag{13}$$

where θ_0 and ϕ_0 are the main beam steering angles, and x' and y' correspond to the distances to the origin for each element on x- and y-axes [7].

The equation (13) was used to visualize the array factor of an uniformly excited planar 8×8 rectangular array and the result is shown in Figure 6. As can be seen in

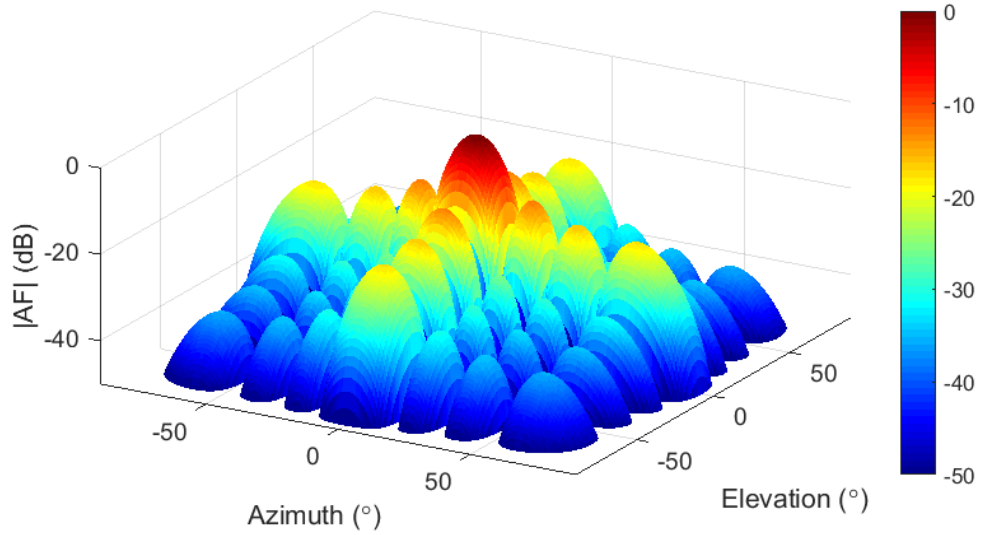

Figure 6: Normalized array factor of planar rectangular 8×8 array with element spacing of $\lambda/2$.

the figure, the array factor of a planar rectangular array is comparable to the array factor of a planar array on the elementary E- and H-planes. It can be also seen, that the side lobes with the most impact are on the these planes. The side lobes between these planes are far smaller than the side lobes on them. The same behavior is also applicable to grating lobes, which restrict the maximum physical size of an element in a phased array and are discussed in the next section. In arrays with different grid the array factor and the behavior of the sidelobes will also be different.

3.2 Grating lobes

Grating lobes are lobes in the array factor of an array antenna identical to the main lobe which might appear in the array factor if the element spacing in an array is too large compared to the wavelength [3]. Usually the emerging grating lobes are a disadvantage as similar amount of energy is transmitted or received from two or more different directions. In radar or sensor applications this could cause ambiguity which is not desired.

Grating lobes are created when the waves from each element constructively interfere at any other direction than the direction of the main lobe. The direction of a grating lobe in a linear array can be calculated for specific wavelength (λ) and element spacing (d) using

$$\frac{d}{\lambda} = \frac{n}{sin(\theta_0) - sin(\theta_{GL})} \tag{14}$$

when n is any integer, θ_0 is the direction of the main lobe and θ_{GL} is the direction of grating lobe corresponding to n [22]. Only the grating lobes emerging at angles between $-90°$ and $90°$ are real and have to be considered when designing an array,

when 0° corresponds to broadside radiation and the main lobe is steered to any angle in the same range. In rectangular grid planar array the grating lobes behave identical to linear arrays when steered in the elementary planes [22]. Between the elementary planes the grating lobes appear at larger angles compared to the elementary planes. Thus, in most cases the equation for the linear array is also applicable to the rectangular grid planar array.

According to (14), Grating lobes do not emerge at any beam steering angles when the element spacing is less than $\lambda/2$. In practice, less than full $\pm 90°$ beam steering is required, in which case the element spacing could be slightly larger.

Let us consider grating lobes with a few example cases. Normalized array factors for two linear arrays are shown in Figure 7. The element spacings in these arrays are $\lambda/2$ and λ, and in both cases the main lobe of the array is steered to 30°. If the element spacing is $\lambda/2$, only one main lobe is visible. When the element spacing in increased to λ, a second main lobe or the first grating lobe emerges at $\theta = -30°$.

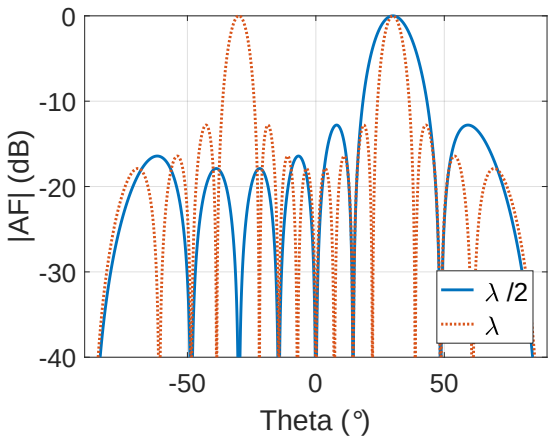

Figure 7: Example of how grating lobes appear in a linear eight element array with element spacing of half a wavelength and one wavelength.

3.3 Mutual coupling

Array factor considers each array element as isolated, isotropic radiator. In practice the elements in an antenna array couple to each other as shown schematically in Figure 8. Therefore elements in an array behave differently than isolated elements. The mutual coupling between the elements in an array antenna influences the impedance and the radiation pattern of each element. The impedance will also vary as a function of the scan angle.

3.3.1 Active element impedance and active reflection coefficient

Active element impedance (AEI) or scan impedance expresses the impedance of an array element as a function of scan angle when all the elements in the array are excited [23]. It is difficult to measure in practice as the whole array has to be

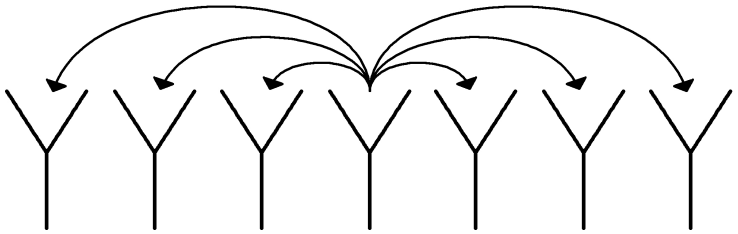

Figure 8: Coupling from one active element to elements with matched termination.

simultaneously excited. Usually, AEI is only used in simulations to evaluate the performance of an element in an infinite array. Infinite array simulations can be used to approximate the performance of an antenna element in a large array.

An array antenna element can be thought as a circuit component in a simple circuit which contains the self impedance of an antenna, the impedance of the environment (or the mutual impedance caused by all the other antenna elements), and the antenna feed voltage generator in series. The voltages (V_n) and currents (I_n) at the terminals of each element in an array which include all the coupling effects can be calculated as

$$\begin{aligned} V_1 &= Z_{11}I_1 + Z_{12}I_2 + \cdots + Z_{1N}I_N \\ V_2 &= Z_{21}I_1 + Z_{22}I_2 + \cdots + Z_{2N}I_N \\ &\vdots \\ V_N &= Z_{N1}I_1 + Z_{N2}I_2 + \cdots + Z_{NN}I_N \end{aligned} \tag{15}$$

where V_n and I_n are the voltage and current in the port of the element n when the mutual coupling is taken in to account, Z_{nn} is the self-impedance of the nth element, and Z_{nm} ($= Z_{mn}$) is the mutual impedance between elements n and m when rest of the elements are terminated to open-circuit [7].

The input impedance of the nth element, i.e., the AEI which takes into account all the coupling in an array can be calculated using 15

$$Z_n = \frac{V_n}{I_n} = Z_{n1}\frac{I_1}{I_n} + Z_{n2}\frac{I_2}{I_n} + \cdots + Z_{nN}\frac{I_N}{I_n} \tag{16}$$

This demonstrates that the input impedance of an element in a phased array changes as a function of the beam steering angle as phase of the currents in all elements are controlled to steer the beam.

From the perspective of the antenna designer, the scattering parameter presentation of the effects of coupling makes more sense as scattering parameters are more commonly used, can be quantified more easily, and can be directly measured with vector network analyzer (VNA). The S-parameters of the first element in a two element array can be expressed with the self-impedances and the mutual impedances between the elements as

$$S_{11} = \frac{(Z_{11} - Z_0)(Z_{22} + Z_0) - Z_{12}Z_{21}}{(Z_{11} + Z_0)(Z_{22} + Z_0) - Z_{12}Z_{21}} \tag{17}$$

$$S12 = \frac{2Z_0 Z_{12}}{(Z_{11} + Z_0)(Z_{22} + Z_0) - Z_{12}Z_{21}} \tag{18}$$

where S_{11} is the active reflection coefficient (ARC) and S_{12} is the mutual coupling. Z_0 is the characteristic impedance of the antenna feed lines, Z_{11} and Z_{22} are the self impedances, and Z_{12} and Z_{21} are mutual impedances which are same due to the reciprocity of antennas. [7], [24]

3.3.2 Active element pattern

The radiation pattern of an antenna element in an array is usually different than the radiation pattern of the similar isolated element. The difference is caused by the mutual coupling between all the elements in the array. Some of the power fed to one element will be radiated through other elements in the array due to this coupling [25]. Radiation pattern of a single array element which takes the mutual coupling, including the scan blindness, into account is known as the active element pattern (AEP) or scan element pattern [7], [22].

In an infinite array, the environment each element sees is identical and thus the AEP of each element is identical and it is directly related to the active reflection coefficient and the gain of isolated element. The relation in an uniform planar array is

$$G_{ae}(\theta, \phi) = G_0(\theta, \phi)[1 - |\Gamma(\theta, \phi)|^2] \tag{19}$$

where $G_{ae}(\theta, \phi)$ is the AEP, $G_0(\theta, \phi)$ is the gain of an isolated element, and $\Gamma(\theta, \phi)$ is the active reflection coefficient [25].

In actual case, the AEP of every element is slightly different. Close to the middle of a large array where the environment each element sees is almost identical, the AEP of any element is also almost identical [25]. At the edge of an array, the environment an element sees is completely different as only half or less of the neighboring elements a center element would see are present. Thus the AEP of an edge element might be vastly different to an element inside the array.

Many arrays are large and most of the elements in large arrays are inside elements with similar radiation environment. Thus, the AEP of a middle element is sufficient for approximating all the array elements. [25] There are numerous advantages using this approach for studying array characteristics as the AEP of a middle antenna element or an element in infinite array can be used to approximate the radiation characteristics of large array antennas. For example, the gain of the array at any angle is directly related to the gain of the AEP in fully excited array at the same angle and the number of array elements

$$G_a(\theta_0, \phi_0) = NG_{ae}(\theta_0, \phi_0) \tag{20}$$

where N is the total number of elements [25]. This means that the HPBW of the AEP is effectively the angular space in which the main lobe of the array can be steered without loosing more than 3 dB of the gain. Similarly, the basic pattern multiplication can be used to generate the radiation pattern of an array when the

AEP is known and the array factor can be calculated. The radiation pattern is calculated as

$$F(\theta, \phi) = G_{ae}(\theta, \phi) f(\theta, \phi) \tag{21}$$

where f is the array factor of the array and F is the total approximated radiation pattern of the array [7].

The AEP can be obtained by exciting one element in an array where other array elements are terminated with matched loads [3]. This can be simulated quite easily in many of the commercial microwave simulation softwares either in infinite array or in the actual array structure. The infinite array simulation can be performed in a software which supports use of periodic boundary condition. Compared to a large array simulation, simulations with the periodic boundary conditions are faster as only one actual element has to be simulated. Most benefit from AEP is received in measurements of an array, as the AEP can basically be measured while feeding only one center element in reasonably large array rather than building the full array with complex feed network. This way the evaluation of the full array performance is easier and more cost efficient.

3.4 Array gain

The maximum directivity of an aperture radiating to one half space is defined as

$$D_{MaxCell} = \frac{4\pi}{\lambda^2} A_{cell} \tag{22}$$

where A_{cell} is the area of one antenna cell or the grid. For example, if the side of a square aperture is half of a wavelength the maximum directivity would be π ($\approx$ 5 dBi). The maximum directivity of an N-element array antenna can be calculated the same way or multiplying the gain of the element by the number of elements like

$$D_{MaxArray} = \frac{4\pi}{\lambda^2} N A_{cell} = \frac{4\pi}{\lambda^2} A_{array} \tag{23}$$

where A_{array} is the area of the array. [7]

The realized gain, which is the actual gain that an element or an array antenna can achieve is calculated by taking the reflection coefficient and aperture efficiency into account, and it can be expressed as

$$G^R = \epsilon_L (1 - |\Gamma|^2) D_{MaxArray} \tag{24}$$

where ϵ_L is the aperture efficiency and Γ is the reflection coefficient [3]. On the other hand, if the AEP of an element in an infinite or large array is simulated or measured, the approximate maximum gain to any steering angle of a large array can be calculated as a product of the array factor and the AEP as shown in equation (21). [7], [25]

4 Simulated structures

The target objectives for antenna performance are defined at the beginning of the project. The specifications are used to define the possible suitable structures to be studied and the direction of the optimization. The requirements are:

- 2 linear polarizations (vertical and horizontal)
- 26–40 GHz frequency range
- the continuous beam steering range ($\theta = 0° - 60°$) $\times$ ($\phi = 0° - 360°$)
- active reflection coefficient < -10 dB.

A single antenna unit cell is required to contain the whole antenna element including both polarizations and the underlying microelectronics including phase and amplitude control or D/A and A/D converters for each element. Single unit cell could include, for example 1×1, 1×2 or 2×2 antennas and an IC to control them. In addition, the antenna array should be scalable so that smaller sub arrays could be combined to form a larger array.

The antenna element size is determined by the emergence of grating lobes. The spacing between radiating elements should be no greater than $\lambda/2$ at the highest operation frequency. When the spacing is exactly $\lambda/2$, half of the first grating lobe arises at 40 GHz when the beam is steered to $\theta = 90°$. The maximum spacing for the antenna elements used in this study is 3.75 mm, which corresponds to the half wavelength at 40 GHz.

The general structure of an antenna unit, array sub element, or the whole array on z-axis can be thought to have three separate components. The antenna structure, the ICs, and the support structure are shown in Figure 9. The implementation of the ICs close to the antenna element is critical in order to decrease the length of the signal path between the antenna and the IC. A short signal path between the IC and antenna allows for more simple feed network and enables low losses. The antennas and ICs are attached to the support structure which also includes the signal paths in the form of microstrips, slotlines, or vias between the antennas and ICs and the data lines to the ICs.

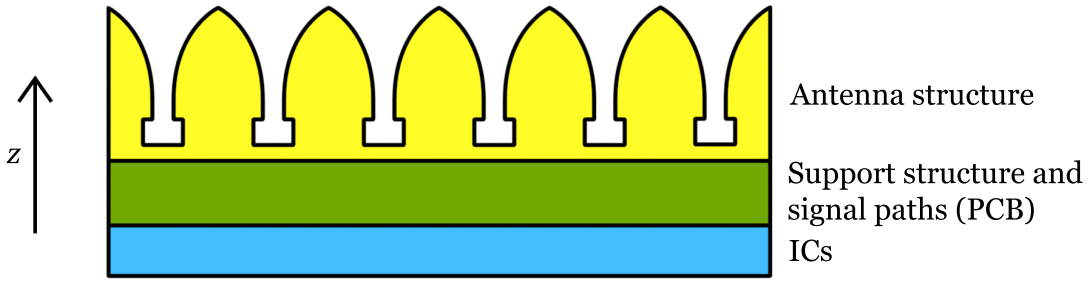

Figure 9: Illustration of a vertical cut of the structure.

Two different antenna types were selected to be studied more thoroughly in simulations. The stacked microstrip patch antenna and the flared-notch or Vivaldi antenna. The flared-notch antenna was later divided into two different implementations.

The stacked microstrip patch antenna element is presented in section 4.2. The flared-notch structures are presented in sections 4.3 and 4.4. The first Vivaldi element type has a more traditional profile. In the second element, the slotline before the exponential flare is meandered and turned 90° in an effort to simplify the feeding.

4.1 Simulation methods

The antenna geometries are simulated and optimized with the frequency and time domain solvers in CST Microwave Studio [26], which is a commercial EM-simulation software. The frequency domain solver is used to acquire access to the unit cell boundary condition. Unit cell boundary condition is periodic boundary condition which allows the simulation of an antenna in an infinite array configuration with faster simulation time compared to a large array in time domain solver as only one actual element has to be meshed and simulated. It is based on Floquet's theorem which states that an infinite regular structure will have the same field in each cell except for the exponential multiplier and the fields can be expressed as a set of orthogonal propagating modes [22]. Using this method also solves the active reflection coefficient (ARC) and active element pattern (AEP) automatically when the beam steering angles are swept as variables [27]. All of the structures are first simulated with unit cell boundary condition and the performance of each antenna is verified for sufficient ARC and the AEP is checked to verify that no scan blindness occurs inside the frequency-scan volume. The performance of an 8×8 array based on each studied element is approximated by multiplying the AEP with an array factor of the 8×8 array.

The structure which is determined to be the most suitable, when considering the manufacturability and the performance, is then simulated in time domain solver in the 8×8 array in which some elements in the middle and edges are excited while the rest of the elements are terminated in matched load. The results of the 8×8 array are compared to the performance which was previously simulated in an infinite array. The 8×8 array is constructed so that it could later be combined with a prototype PCB, manufactured and the performance measured to determine if the manufacturing of such elements is viable in larger volume and if the performance of the related array is comparable to the simulated performance.

4.2 Stacked patch array

The operation of stacked patch antennas was discussed in section 2.2.1. Based on the literature study, stacked patch element was chosen to be simulated and optimized for Ka-band. The structure presented here is only simulated as a single polarized structure as the single antenna element at Ka-band is quite small and it might be challenging to implement feed similar to the structure presented in [17], in the first prototype.

4.2.1 Structure

A 3D model of the stacked patch element is shown in Figure 10. The element is constructed from the ground plane, the main and secondary microstrip patches above the ground plane, and the microstrip feed which is coupled to the primary patch through the aperture in the ground plane. The microstrip feed is terminated to the stub which is more visible in Figure 11b. A low loss dielectric is used between the different copper layers. The structure is not ideal considering the specifications as the aperture coupled feed is large compared to the overall size of the element and there is no space for the second polarization.

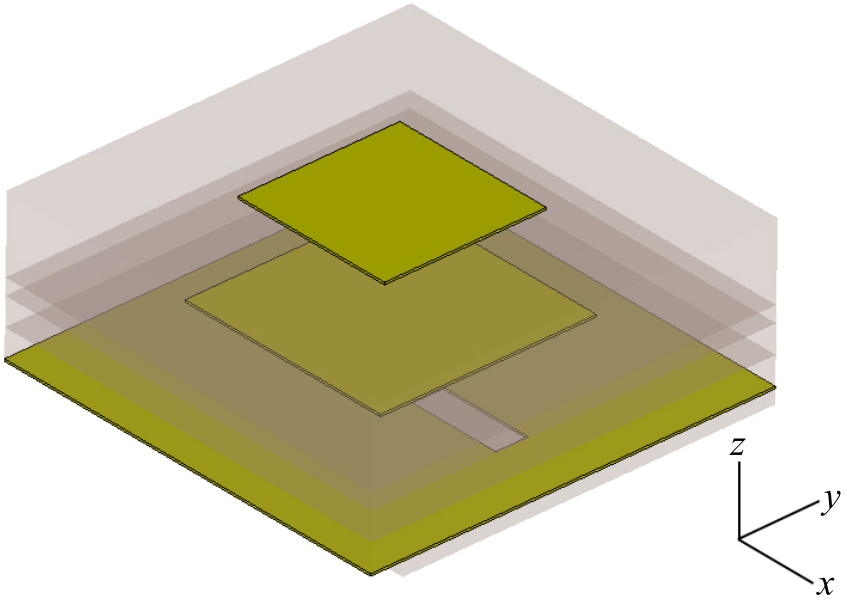

Figure 10: The stacked patch element

.

The design parameters of the structure are shown in Figure 11. The element spacing a is 3.75 mm which corresponds to $\lambda/2$ at 40 GHz which is the maximum element spacing preventing the emergence of grating lobes at any beam steering angle. Although, the element spacing can be slightly increased as the maximum required steering angle is 60°. The main design parameters responsible for the frequency response of the element are the widths of the primary patch b and the secondary patch c, the spacing between the primary patch and the ground plane h_2, and the spacing between the secondary and primary patches h_3. The width of the microstrip d and the thickness of the substrate h_1 defines the impedance of the microstrip line which in this case is approximately 100 Ω. The microstrip is terminated to a short low impedance open-ended stub with dimensions i and j to match the microstrip and the aperture. The aperture used as a resonator to increase the bandwidth and to couple the energy from the microstrip to the microstrip patches is placed in the middle under the element. The size of the aperture defined by e and f was optimized through numerical simulations to effectively couple the energy from the microstrip line to the microstrip patches. The width is quite large to allow the microstip to

couple to the patch elements well which increases the difficulty to implement two polarizations in one element. Rogers RT5880 is used in between the metal layers due to its low loss (tan $\delta = 0.0009$@10 GHz) and low dielectric constant ($\epsilon_r = 2.2$).

MODEL DIMENSIONS (mm)

a	b	c	d	e	f	h_1	h_2	h_3	i	j
3.75	2	1.5	0.1	2.5	0.3	0.127	0.5	0.825	0.4	0.7

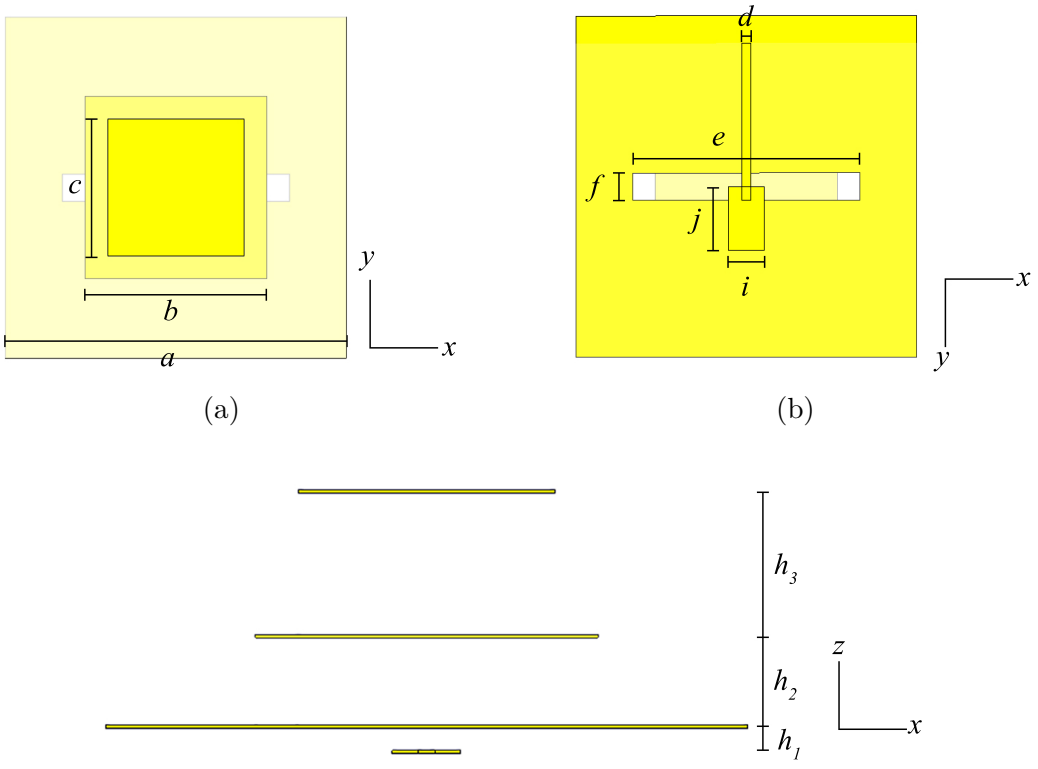

Figure 11: (a) the top profile, (b) the bottom profile and (c) the side profile of the stacked patch element with relevant design parameters.

4.2.2 Simulation results

The simulation model described in the previous section was simulated in an infinite array using the frequency domain solver, unit cell boundary conditions on x- and y-boundaries and Floquet port on boundary above the element. The antenna was fed using waveguide ports coupled to the microstrip line under the whole structure. Only one polarization is included to the simulations as the feed used in this structure is quite large and both polarizations do not fit under the patch.

The active element impedance of one polarization element is presented at 26, 29, 32, 34, 37, and 40 GHz in Figure 12. The beam steering angles are presented on x- and y-axes and the value of ARC is presented as a color in a point. θ represents the

steering away from broadside and ϕ represents the steering around the broadside axis. A line for the $-10\,\mathrm{dB}$ value is presented in the figures for easier evaluation of the results. The ARC is inside the specifications at only around 29 GHz, where it is better than $-10\,\mathrm{dB}$ at any beam steering angle. At lower frequencies the ARC exceeds $-10\,\mathrm{dB}$ when $\theta > 50°$ and ϕ is close to 90°. Above 29 GHz the ARC exceeds $-10\,\mathrm{dB}$ generally at all ϕ when θ is steered 30° to 50° away from broad side. The total efficiency of the antenna structure when beam is steered to broadside and 60° on *E*-, *H*-, and *D*-planes is shown in Figure 13. When the antenna is used for broadside radiation the efficiency is above 90% through the whole frequency range. At $\theta = 60°$ steering angles, the efficiency drops below 90% as can be deduced from the ARC figures. At *H*-plane, the efficiency is extremely low at 39 GHz which is caused by scan blindness.

Figure 14 shows the normalized active element patterns of the structure for *E*- and *H*-plane at 26, 33, and 40 GHz. Only the elementary planes are presented but the shape of the pattern can be interpolated between the *E*- and *H*-planes. At 40 GHz, the *H*-plane radiation pattern is degraded due to scan blindness. The most severe scan blindness occurs at 39 GHz at $\theta = 60°$ and the effect is visible through out the higher frequency band at steering angles from $\theta = 20°$ to 60° close to the *H*-plane. The HPBW of the element is about 120° at 26 GHz but it begins to decrease as the frequency increases. At 33 GHz the HPBW is decreased to 110° and at 40 GHz the *H*-plane HPBW is decreased to about 85° due to the scan blindness.

The planar structure is attractive choice due to low overall height which makes it ideal to be used for example in conformal arrays in aircrafts and ships. Unfortunately, it seems to be quite susceptible to scan blindness due to the larger spacing between the aperture and the patches. Additionally, the feed structure studied here does not allow implementation of both polarizations in one array element. It could be possible to implement the more complex dual polarized feed structure with further research.

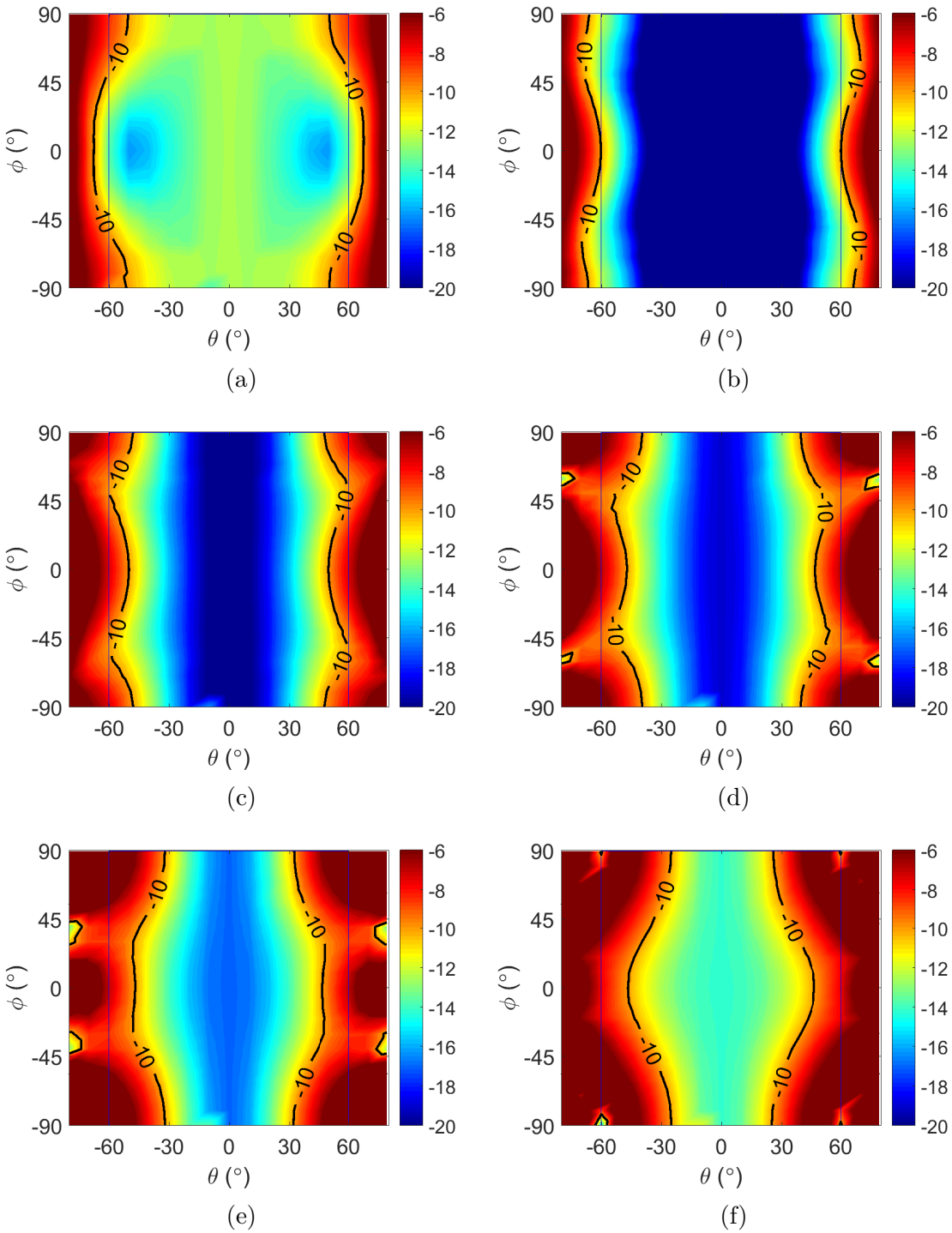

Figure 12: Active reflection coefficient of the stacked patch element in an infinite array at a) 26 GHz, b) 29 GHz, c) 32 GHz, d) 34 GHz, e) 37 GHz, and f) 40 GHz.

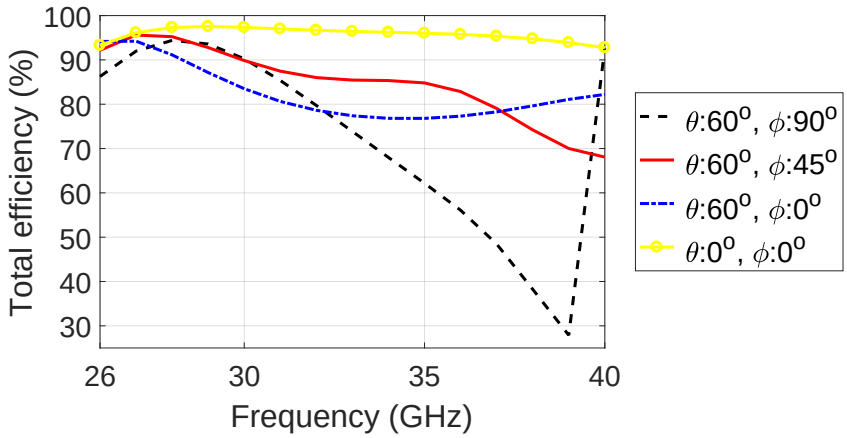

Figure 13: The efficiency of the stacked patch array antenna at different steering angles.

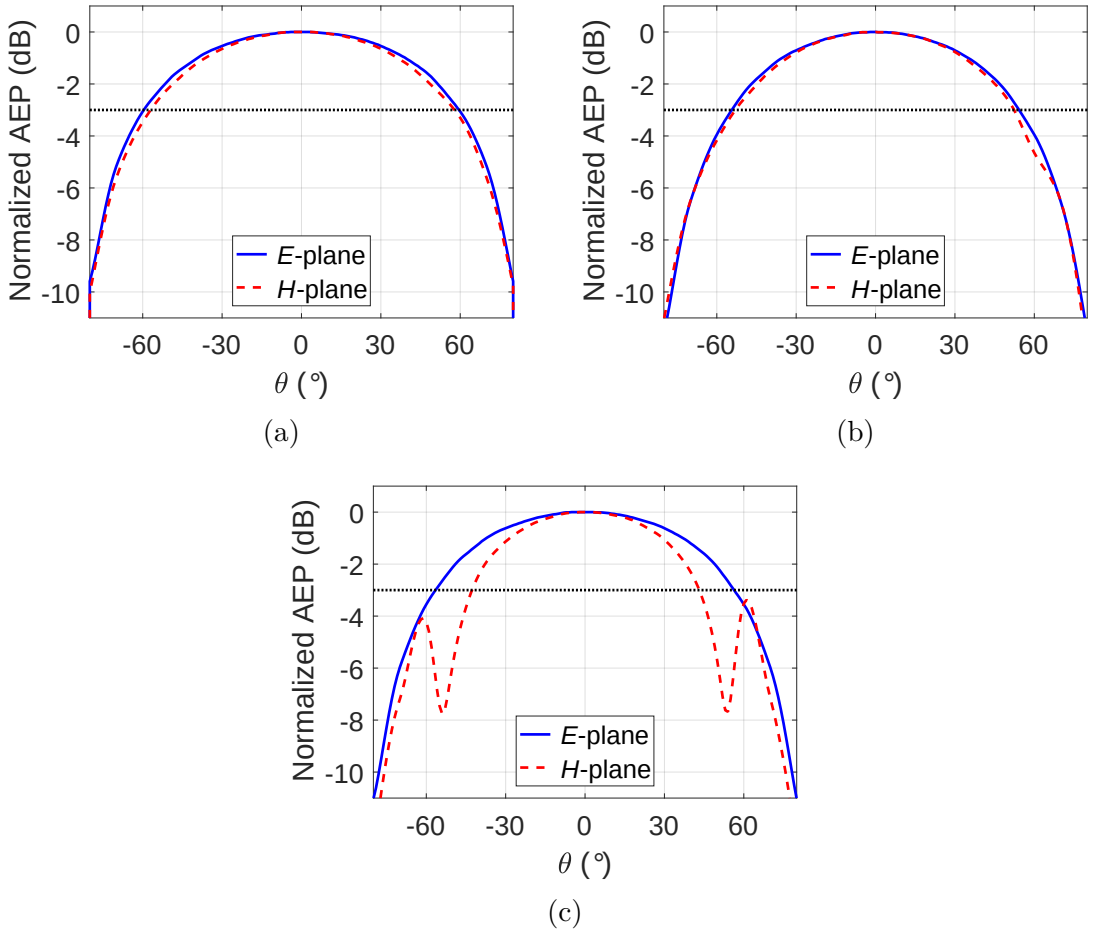

Figure 14: Normalized active element pattern of the stacked patch element in an infinite array at (a) 26 GHz, (b) 33 GHz, and (c) 40 GHz.

4.3 Rectangular cone array on PCB

This structure is based on the broadband antenna array introduced by Holter for 6 – 18 GHz [28], [29]. The profile of antenna array element presented in the paper is similar as shown in Figure 15 and each cone is rotationally symmetric around z-axis. An electrical conductor is routed through a hole in the base of the cone forming a coaxial feed which is rotated 90° at the base of the flare and have galvanic connection to the next cone. The antenna element presented here is made rectangular due to the limitations in the size of the element set by the higher operation frequency.

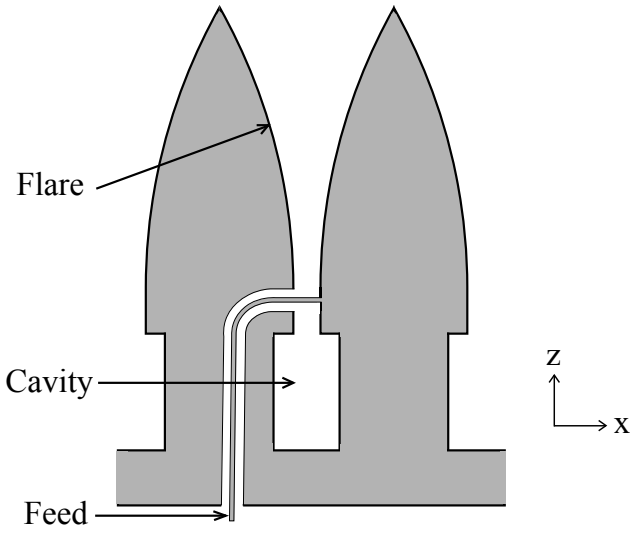

Figure 15: Basic illustration of a flared-notch antenna structure presented in [29].

4.3.1 Structure

The antenna array is constructed from rectangular cones placed on a xy-plane the point of the cone facing the direction of the radiation as shown in Figure 16. A single cone, which was also the unit cell for the simulations, can be seen in Figure 16a. Two similar cones, when diagonally placed next to each other, form a single radiating element between the cones. The cones are constructed from two parts as shown in Figure 16b. The top cones are fully metallic structures and the bottom part is a milled PCB in which the sides of the cones are metal coated. Only the dielectric between the cones and small part on the dielectric from where the strip line enters the slot between the cones do not have the metal coating. The signal is routed inside one cone and galvanically connected to the other cone over the cavity.

Figure 16b shows a square 4×3 array in which the metallic cone structure is separated from the PCB containing the signal paths and the cavities. This type of structure does not completely follow the requirements as it is relatively hard to include the whole radiating element inside one physical unit cell due to the strip lines and the vias inside the cones. Consequently, the structure is also not completely compatible with the specifications regarding the scalability because the unit cell border cuts the feeds in half between the cones. This means that the whole array of

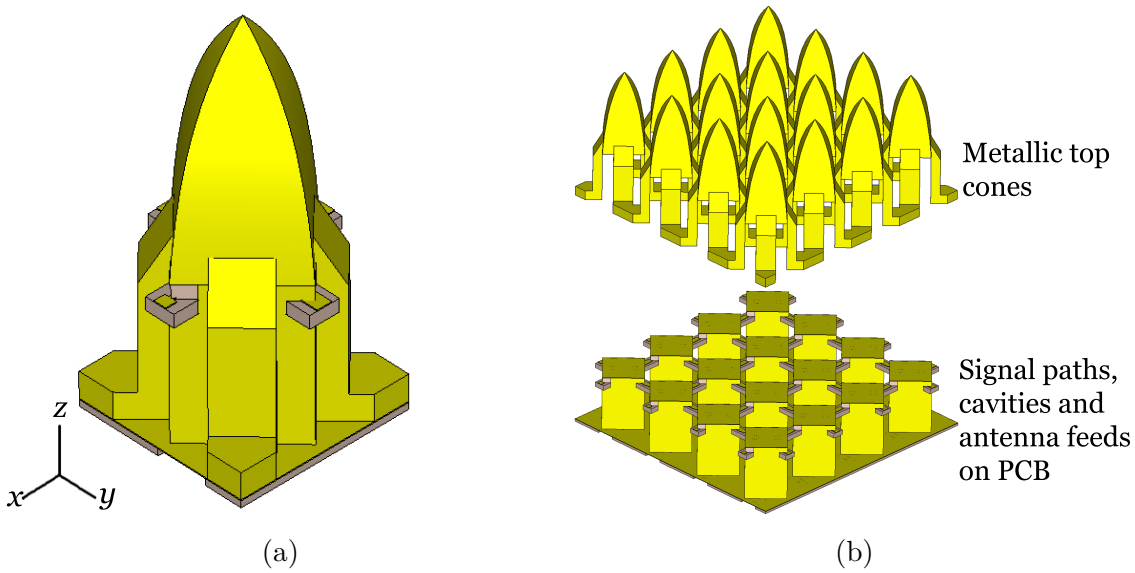

(a) (b)

Figure 16: (a) A single dual polarized unit cell antenna element which is used to simulate and calculate ARC and AEP in the infinite array. (b) A 4×3 array of dual polarized elements when the metallic top cones are separated from the PCB.

these elements would have to be manufactured to correct size or there would be one row of passive elements in the polarization perpendicular to the sub array border.

The top view and the profile of the element with the most important design parameters are shown in Figure 17. The element spacing a is slightly smaller than $\lambda/2$ which increases the angular space between the main lobe and the first grating lobes decreasing the possible problems caused by the arising grating lobe when the main lobe is steered to the maximum. The height of the antenna structure b without PCBs behind the element is 7.1 mm which is the result of optimizing the height of the metal top cone c and the length of the cavity d. The profile of the side of the square is defined by R in Equation (5) with rate R. The opening rate of the corner which is the actual radiating element is higher. The impedance and the matching from stripline to the antenna is defined by the width between the cone corners e. The matching is further improved by increasing the width of the copper line in the transition from stripline inside the cone to the exponential slotline radiator h and g. The size of the connecting arms between the top cones (i and j) is kept as small as possible to avoid any major decrease in performance.

The design parameters of the signal paths inside the cones are presented in Figure 18. The impedance of the transmission lines is optimized to match that of the slot of the antenna and the width of the lines q are minimized to fit the small structure by using thin substrates with small dielectric constant. Rogers RT5880 is used as the substrate due to its small dielectric constant and low dielectric losses even at high frequencies ($\epsilon_r = 2.2$, $\tan\delta = 0.0009$@10 GHz). The impedance of the 100 μm line is approximately 100 Ω. The corresponding substrate thickness for microstrip line is 0.127 mm and for stripline 0.256 mm. Microstrip is used under the whole structure and fed in the simulations with a wave port. Stripline is used inside the

MODEL DIMENSIONS (mm)

a	b	c	d	e	f	g	h	i	j	$R_{\frac{1}{\text{mm}}}$
3.42	7.1	4.2	2.4	0.45	2.1	0.3	0.25	1	0.5	0.6

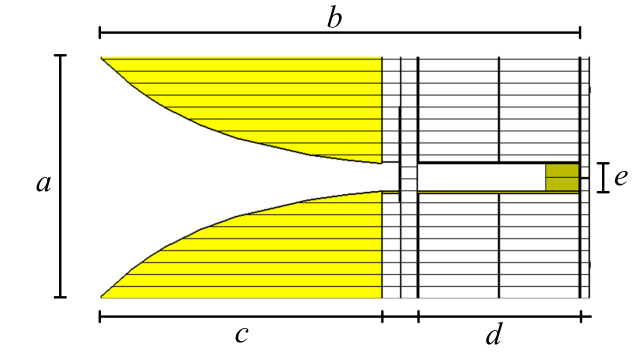

(a)

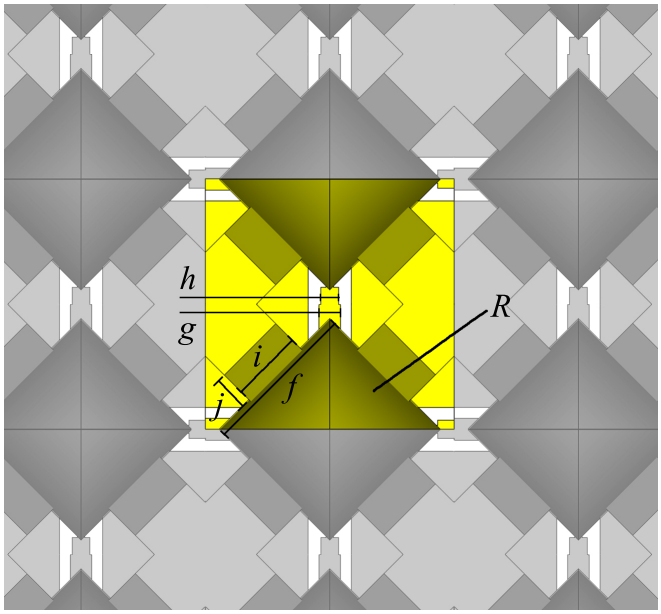

(b)

Figure 17: (a) A profile of a single radiating element of the structure and (b) a top view of the element with relevant design parameters.

structure on the layer which contains the feed. The signal is transferred from the bottom microstrip to the striplines in the middle of the structure through vias. The impedance of the vias are tuned with the diameter of the via k, the radius of the circular cut-out in the ground layers p, and the spacing between the signal and ground via (n and m). The diameter of the ground via l is not critical and is chosen larger to ease the manufacturing.

MODEL DIMENSIONS (mm)

k	l	m	n	p	q
0.2	0.4	0.55	0.65	0.45	0.1

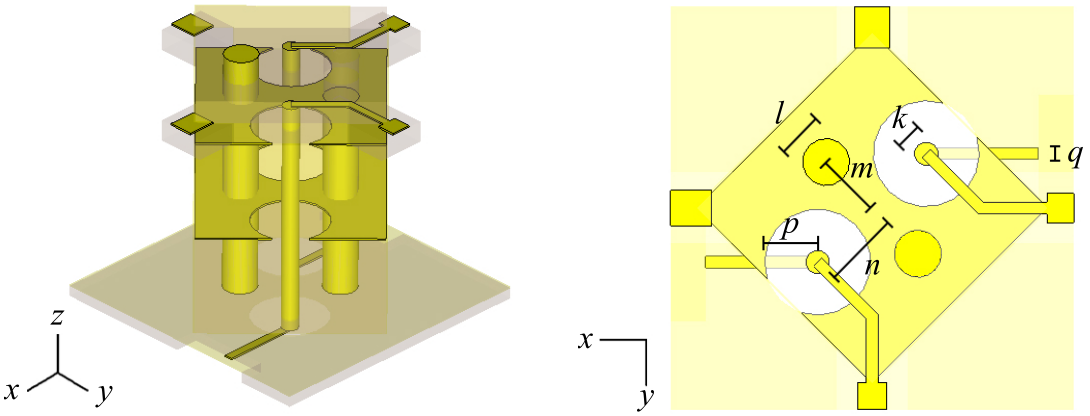

(a) (b)

Figure 18: (a) A 3D view of the signal paths from the bottom of the PCB to the antenna feed and (b) a top view of the same structure with relevant design parameters.

4.3.2 Simulation results

The simulation model described in the previous section is simulated in an infinite array using the frequency domain solver, unit cell boundary conditions on x- and y-boundaries and Floquet port on the boundary above the element. The antenna was fed using waveguide ports coupled to the microstrip line under the whole structure. Due to the inclusion of all relevant transitions in the structure (microstrip to via, via to stripline, and stripline to the radiator) the simulation results should accurately present the performance and losses of such structure. The simulated array also includes both vertical and horizontal polarization.

The active element impedance of one polarization element is presented at 26, 29, 32, 34, 37, and 40 GHz in Figure 19. The beam steering angles are presented on x- and y-axes and the value of ARC is presented as a color in a point. θ represents the steering away from broadside and ϕ represents the steering around the broadside axis. A line for the -10 dB value is presented in the figures for easier understanding. The ARC is better than -10 dB almost throughout the frequency range from 26 to 40 GHz at all scanning angles (ϕ : 0° – 360°, θ : 0° – 60°). At the low end of the frequency range when θ is 60° and ϕ is around ±90° the performance is slightly worse than -10 dB. Between 28 and 37 GHz, there is at least one decibel margin at all scanning angles and at 40 GHz the performance is better than -8.5 dB when θ is steered 60° and ϕ is ±50–90°. The worst observed ARC to the broadside direction is at 26 GHz approximately -11.5 dB.

Figure 20 shows the cross polarization. It is good through out the frequency range and corresponds well with previous studies on flared-notch arrays [21]. The cross polarization is generally better than -25 dB and slightly higher on the D-planes. At 40 GHz the worst simulated cross polarization levels are approximately -15 dB at

D-planes when $\theta > 40°$.

The total efficiency of the antenna structure from 27 to 39 GHz is better than 90% and in the whole range better than 85% as can be seen in Figure 21. In addition to the broadside, the efficiency is also plotted on the elementary E- and H-planes and on diagonal D-plane at 60 degree steering angle.

Figure 22 shows the normalized active element patterns of the structure for E- and H-plane at 26, 33, and 40 GHz. Only the elementary planes are presented but the shape of the pattern varies very little at angles between the E- and H-planes. As the shape of the pattern is almost constant while the angle ϕ is scanned, the approximation of the far field pattern of an array can be expected to also be constant. Thus, it is sufficient to approximate the radiation pattern of an array only, at E-plane for example.

The HPBW of the element is about 120° to all angles ϕ and the gain is already decreased to approximately −10 dB at 80° degrees. Even though the element spacing is sufficiently small so that no grating lobes are generated, the lower gain to angles greater than 60° will greatly suppress the gain of side lobes to those directions. One important observation that can be done from these AEPs is that there is no scan blindness in any beam steering angle.

The radiation pattern of an 8×8 array is approximated by multiplying the E-plane cut of the AEP with the array factor of 8×8 array. The approximated normalized radiation patterns are presented at 26, 33, and 40 GHz in the Figure 23. The radiation patterns, when the array factor is steered 0° and 60° are included in the figures. The side lobe level of the simulated array is approximately −13 dB when the radiation is directed to the broadside direction. When the array factor is steered to 60° the SLL increases slightly to −10.5 dB. This is directly related to the drop in gain in the AEP. Another observation is the slight lag in the beam steering of the array compared to the array factor when steered to extreme angles. When array factor is steered to 60°, the maximum of the radiation pattern is actually only at 56°.

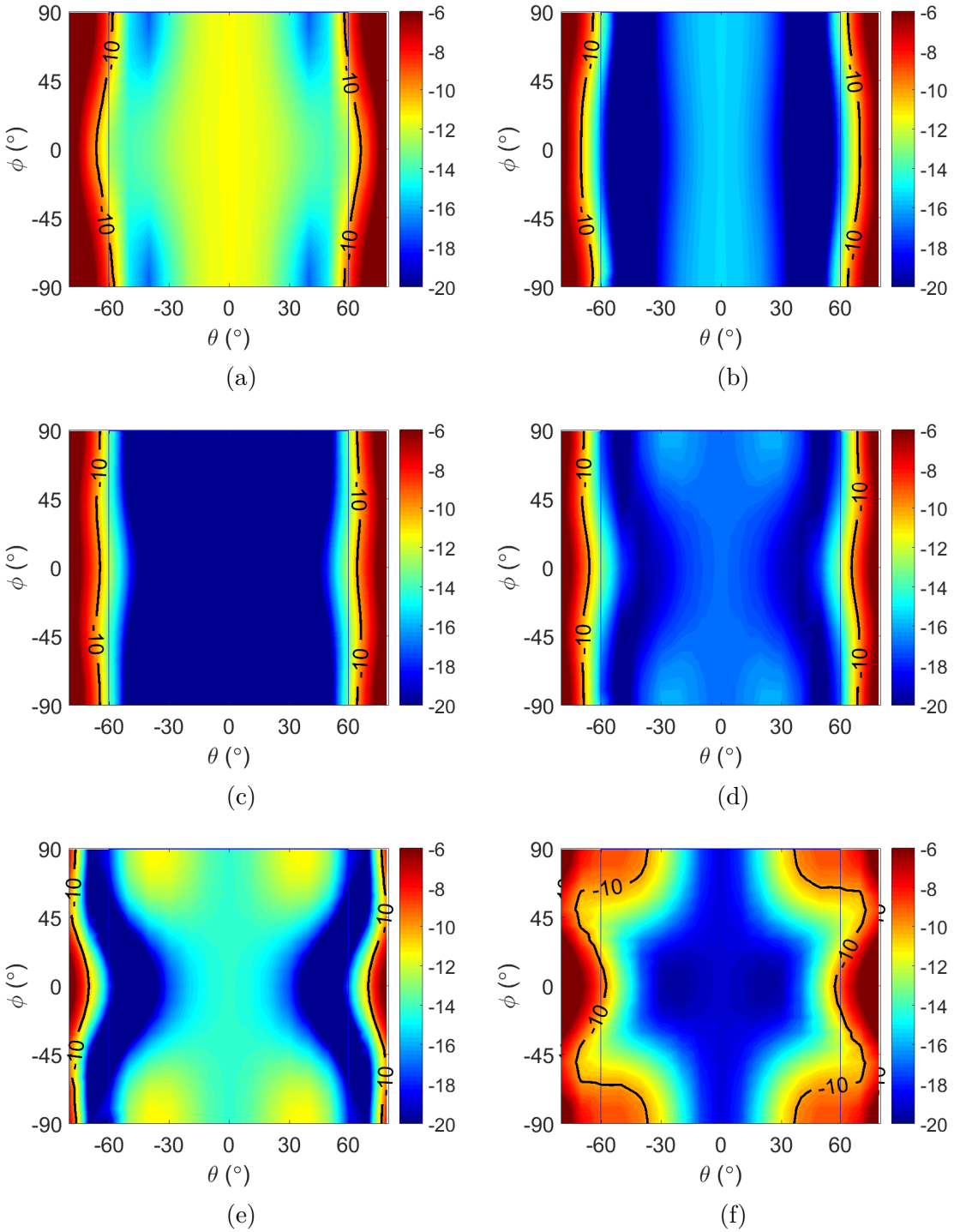

Figure 19: Active reflection coefficient of the rectangular cone element on PCB in an infinite array at a) 26 GHz, b) 29 GHz, c) 32 GHz, d) 34 GHz, e) 37 GHz, and f) 40 GHz.

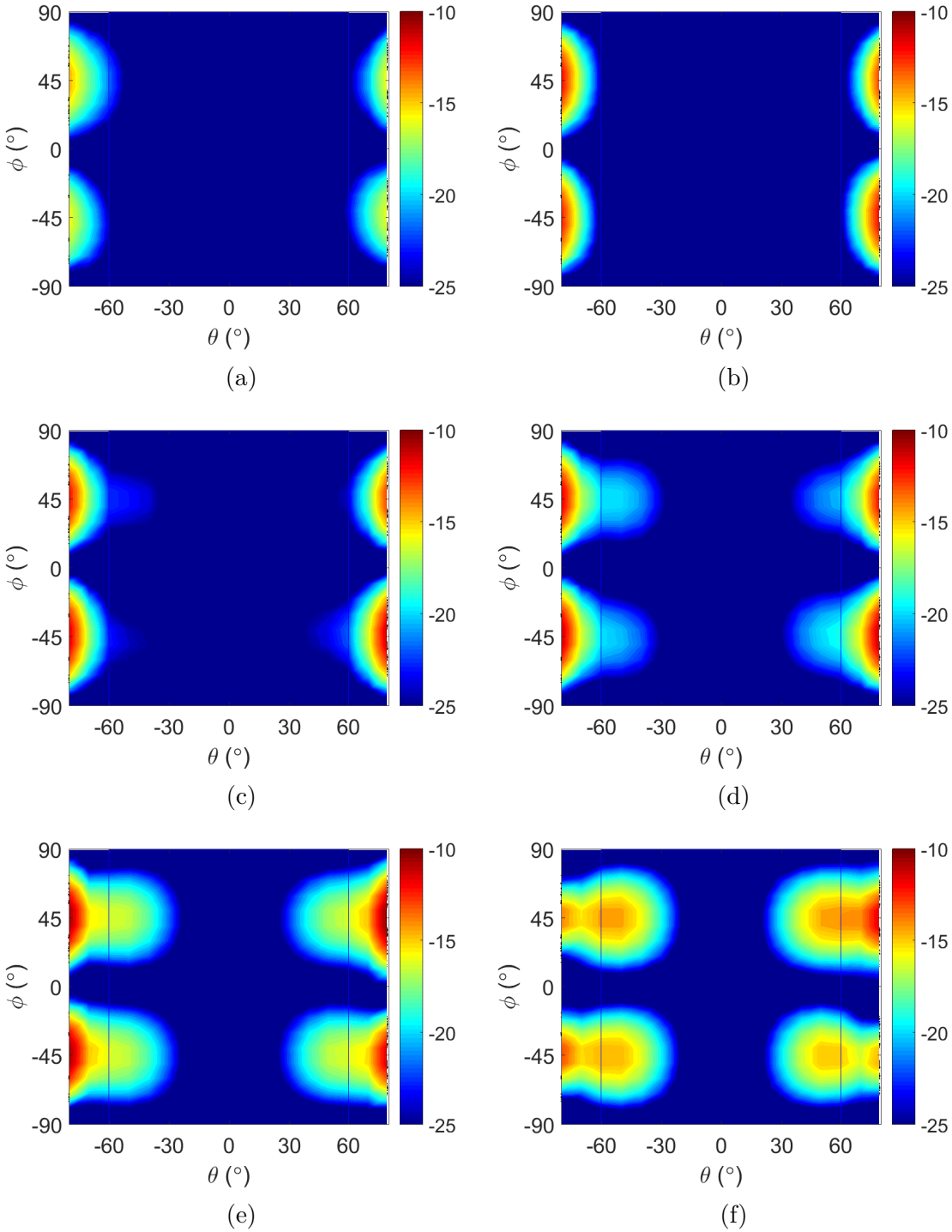

Figure 20: Cross polarization of the rectangular cone element on PCB in an infinite array at a) 26 GHz, b) 29 GHz, c) 32 GHz, d) 34 GHz, e) 37 GHz, and f) 40 GHz.

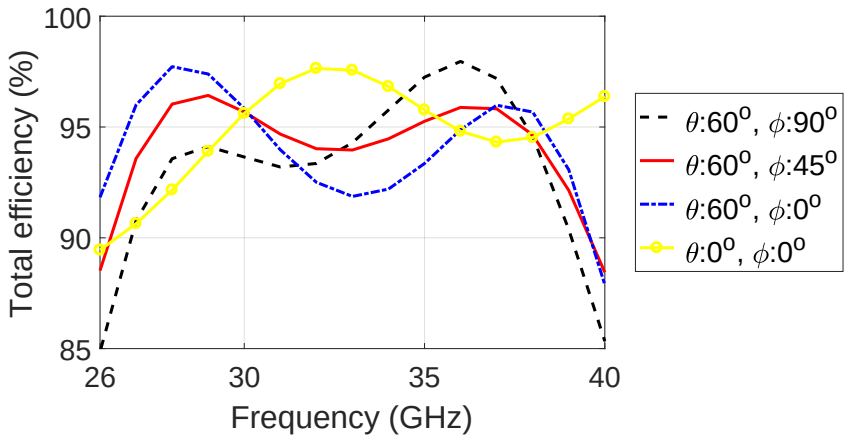

Figure 21: The efficiency of the rectangular cone array at different steering angles.

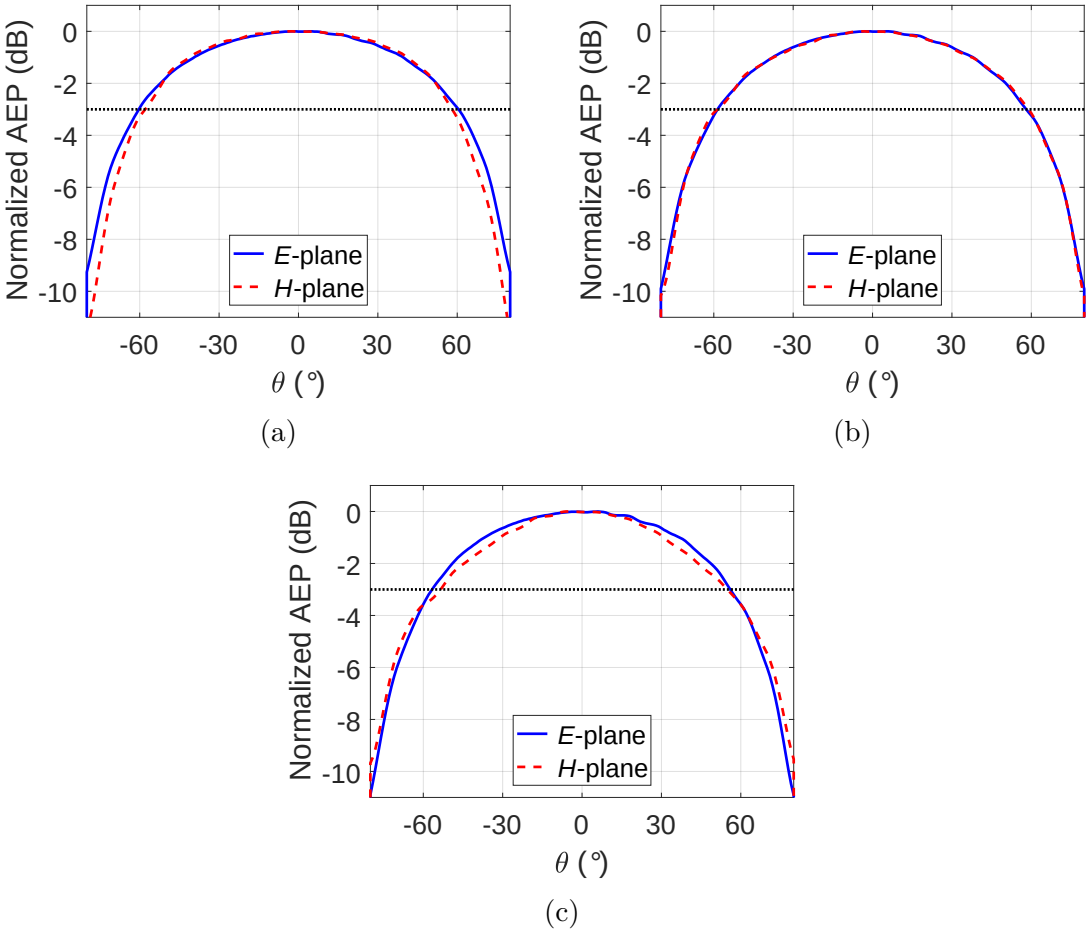

Figure 22: Normalized active element pattern of the rectangular cone element on PCB in an infinite array at (a) 26 GHz, (b) 33 GHz, and (c) 40 GHz.

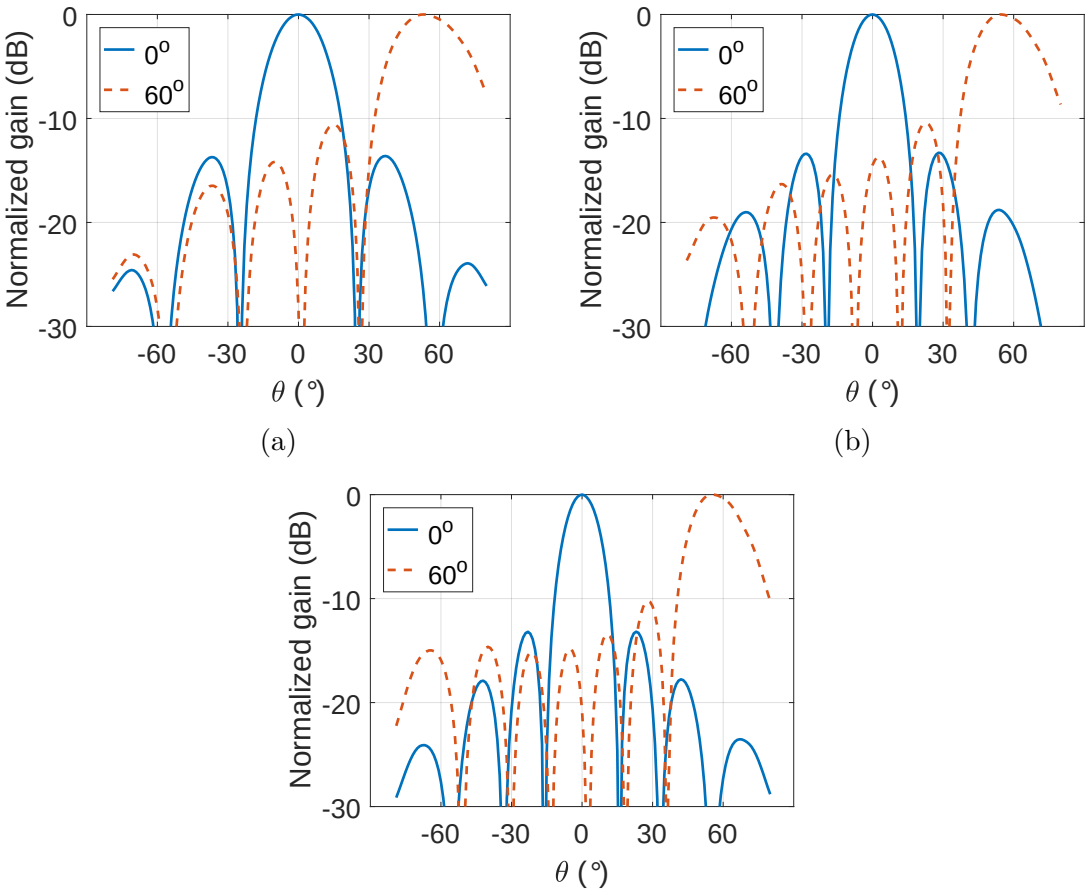

Figure 23: Normalized gain of an 8×8 array approximated from AEP when the array factor is steered to 0° and 60° on E-plane at (a) 26 GHz, (b) 33 GHz, and (c) 40 GHz.

4.4 Bent feed flared-notch antenna

The previous flared-notch structure imposes manufacturing challenges because the cavities machined in the PCB would have to be metal plated and the element is hard to divide into unit cells without braking the feeds inside the cones. To facilitate manufacturing, a bent feed flared-notch antenna was studied. The basic operation of the antenna and the performance are very close to the previous structure but the manufacturing would be easier. The antenna structure could be manufactured using regular milling and wire EDM, or additive manufacturing either by metal plating 3D printed plastic structure or 3D printing with metal.

The structure is based on the ultra-wideband antenna array for 0.7–9 GHz studied by Kindt and Pickles in [30]. In this structure, the feed probe can be implemented along the vertical axis as an attempt to simplify the manufacturing of the antenna feed. The challenges in this type of structure are the possible cross coupling when the cavities are brought closer together and implementation of the cavity and the slot line in the already small space available is difficult.

4.4.1 Structure

For this antenna structure, only copper was used as a material and the underlying feeding network and PCB was omitted. The unit cell simulation structure is presented in Figure 24a. To clarify how this element would appear in an array constructed from such elements, an illustration of a 4×4 array is additionally presented in Figure 24b. The single unit is constructed from two identical elements for two polarizations rotated 90° around the z-axis.

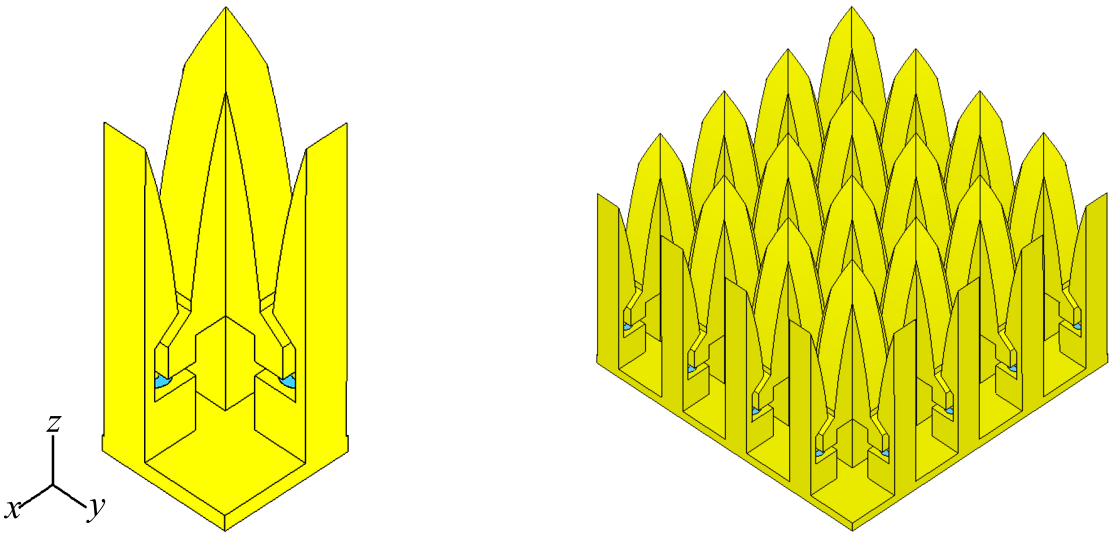

(a) (b)

Figure 24: (a) A single dual polarized unit cell antenna element which is used to simulate and calculate ARC and AEP in the infinite array. (b) A 4×4 array of dual polarized elements.

A more detailed profile of the unit cell with the relevant design parameters is shown in Figure 25. The element spacing of 3.75 mm (Figure 25: a+b) is small enough to allow beam steering to specified angles without invoking grating lobes in an array of such elements. The parameters that have the most impact on the center frequency of the structure are the element spacing (a+b) where b is the thickness of the antenna element, the length of the flare c, the size of the cavity (d and j) and the opening rate for the exponential taper profile R. Parameters for the feed pin diameter h, outer diameter of the coaxial i and the width of the slot f define the input impedance of the antenna. The impedance of the slot requires rigorous calculations [31] but the impedance of the coaxial pin is straight forward to estimate using [32]:

$$Z_0 = \sqrt{\frac{\mu}{\epsilon}} \frac{\ln b/a}{2\pi} \tag{25}$$

when b is the inner diameter of the outer conductor of the coaxial and a is the outer diameter of the inner conductor.

The optimal matching for the feed was solved through simulation. Optimal reflection coefficient was achieved when the impedance of the coaxial feed pin was 83 Ω.

The lengths of the slot line after the 90° bend and before the flare (g and e) and the thickness of the element b are somewhat restricted by the previous parameters but also are part of the optimization for good efficiency. For example, the minimum thickness of the element is restricted by the outer diameter of the coaxial pin and simultaneously increases the available space for the cavity if minimized.

MODEL DIMENSIONS (mm)

a	b	c	d	e	f	g	h	i	j	l	$R_{(\frac{1}{\text{mm}})}$
2.5	1.25	7	2.7	1.5	0.4	0.7	0.2	0.8	0.9	11.2	0.2

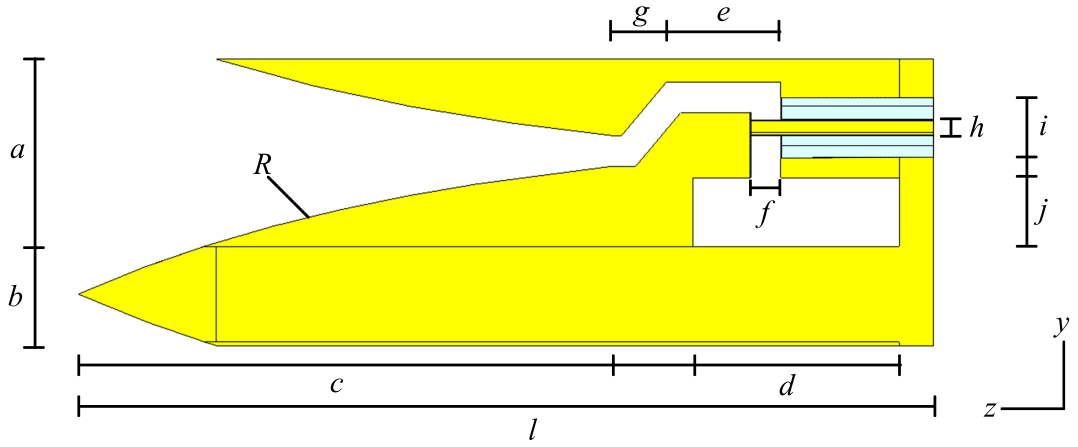

Figure 25: Dimensions of a single unit cell element of the antenna structure.

4.4.2 Simulation results

The simulation model described in the previous section is simulated in an infinite array using the frequency domain solver, unit cell boundary conditions on x- and y-boundaries and Floquet port on boundary above the element. The antenna was fed using waveguide ports coupled to the end of the coaxial pins under the element for each polarization. Because the PCB and transition from stripline or microstrip to the coaxial pin was not included into the simulated structure, it is expected that the performance of the structure with aforementioned components is slightly decreased.

The active element impedance of one polarization element is presented at 26, 29, 32, 34, 37, and 40 GHz as a function of angles ϕ and θ in Figure 26. A line for the -10 dB value is presented in the figures for easier understanding. The ARC is better than -10 dB throughout the frequency range from 26 to 40 GHz at all scanning angles ($\phi : 0° - 360°$, $\theta : 0° - 60°$). At the low end of the frequency range, when θ is 60° the performance is just barely within the specified -10 dB. Between 28 and 37 GHz, there is at least two to four decibel margin at scanning angles and close to the maximum frequency the performance is again just barely above -10 dB when θ is steered 60° in E- or H-plane. The worst observed ARC of -12 dB to the broadside direction is at 29 GHz.

Figure 27 shows the cross polarization which is not symmetric anymore as in the previous structure due to the asymmetric bent feed. The cross polarization is also higher as the cavities and the slot line are closer in the structure. The average cross polarization is between -20 and -17 dB, and -15 dB at its worst.

The total efficiency of the antenna structure from 27 to 38 GHz is better than 90% and in the whole range better than 86%. The total efficiency is presented in Figure 28. In addition to the broadside, the efficiency is also plotted on the elementary E- and H-planes and on diagonal D-plane at 60° steering angle.

Figure 29 shows the normalized active element patterns of the structure for E- and H-plane at 26, 33, and 40 GHz. Only the elementary planes are presented but the shape of the pattern varies very little even at any angle between the E- and H-planes. As the shape of the pattern is almost constant while the angle ϕ is scanned, the approximation of the far field pattern of an array can be expected to also be constant. Thus, it is sufficient to approximate the radiation pattern of an array only, at E-plane for example.

The HPBW of the element is about 120° to all angles ϕ and the gain is already decreased to approximately -10 dB at 80° degrees. Even though the element spacing is sufficiently small so that no grating lobes are generated, the lower gain to angles greater than 60° will greatly suppress the gain of side lobes to those directions. One important observation that can be done from these AEPs is that there is no scan blindness in any beam steering angle.

The radiation pattern of an 8×8 array is approximated by multiplying the E-plane cut of the AEP with the array factor of 8×8 array. The approximated normalized radiation patterns are presented at 26, 33, and 40 GHz in the Figure 30. The radiation patterns, when the array factor is steered 0° and 60° are included in the figures. The side lobe level of the simulated array is approximately -13 dB when the radiation

is directed to the broadside direction. When the array factor is steered to 60° the SLL increases slightly to −10.5 dB. This is directly related to the drop in gain in the AEP. Another observation is the slight lag in the beam steering of the array compared to the array factor when steered to extreme angles. When array factor is steered 60° the maximum of the radiation pattern is actually only at 56°.

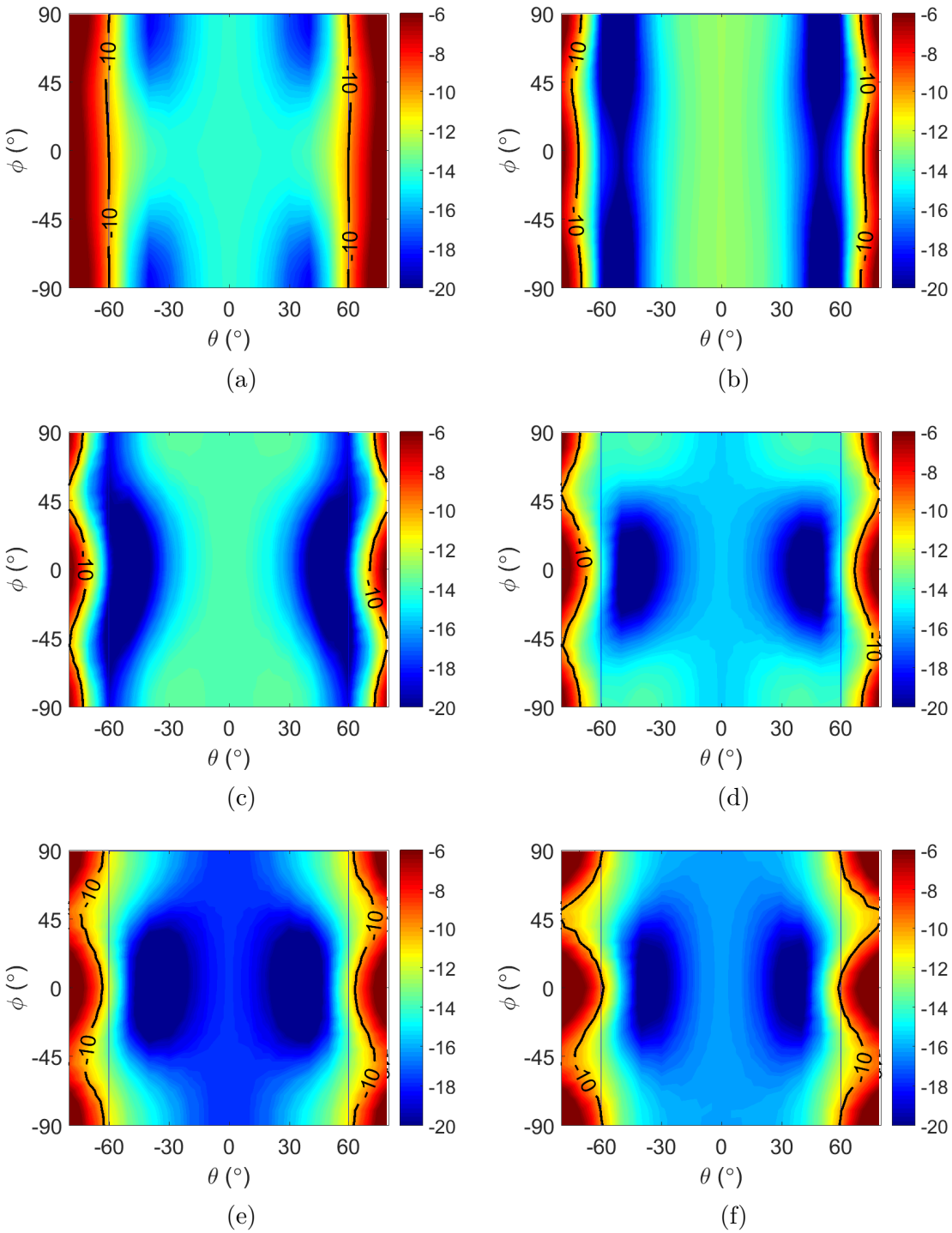

Figure 26: Active reflection coefficient of the bent flared-notch element infinite array at (a) 26 GHz, (b) 29 GHz, (c) 32 GHz, (d) 34 GHz, (e) 37 GHz, and (f) 40 GHz.

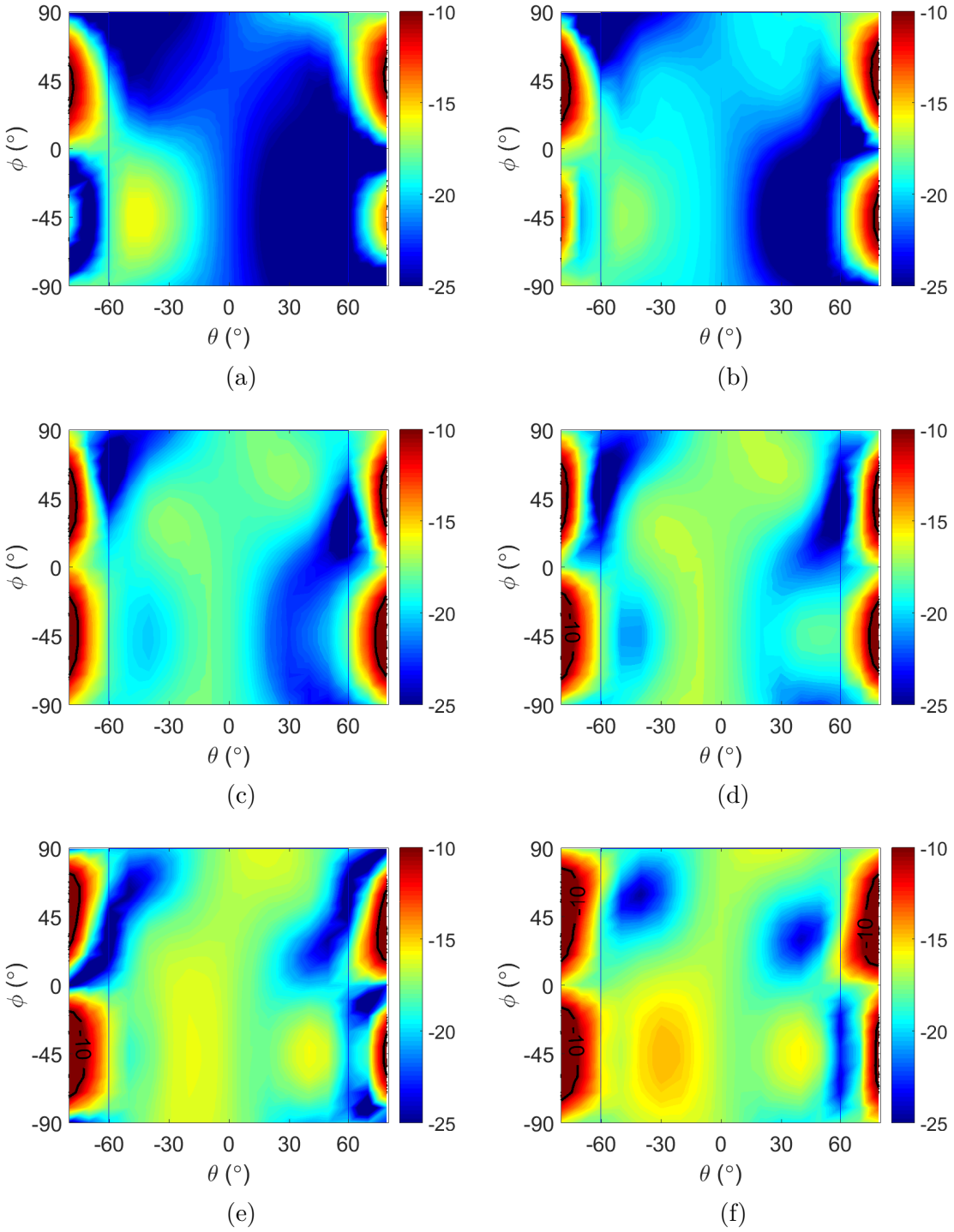

Figure 27: Cross polarization of the bent flared-notch element infinite array at (a) 26 GHz, (b) 29 GHz, (c) 32 GHz, (d) 34 GHz, (e) 37 GHz, and (f) 40 GHz.

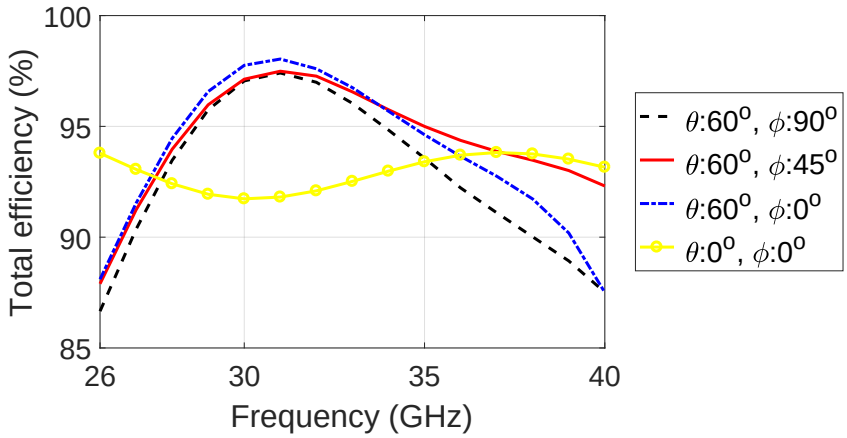

Figure 28: The efficiency of the bent feed flared-notch antenna at different steering angles.

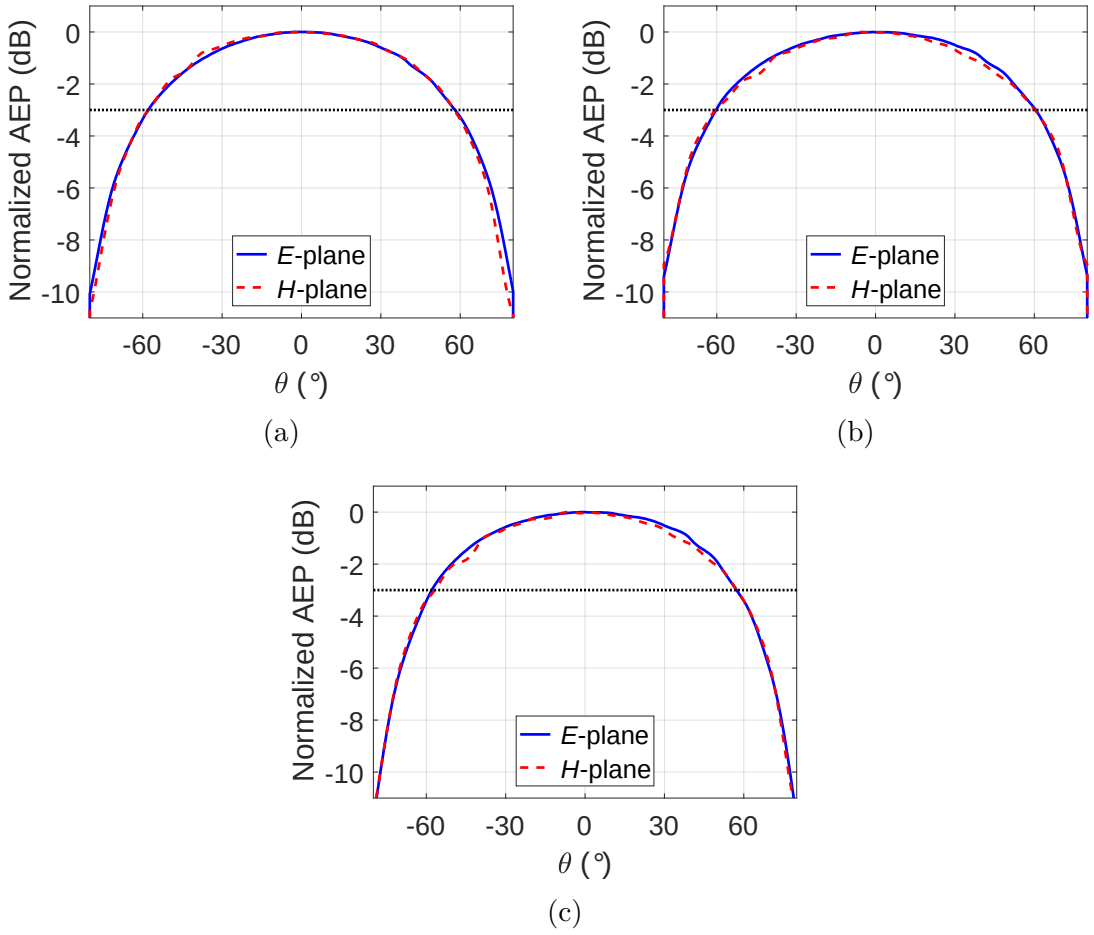

Figure 29: Normalized active element pattern of the bent feed flared-notch element infinite array at (a) 26 GHz, (b) 33 GHz and (c) 40 GHz.

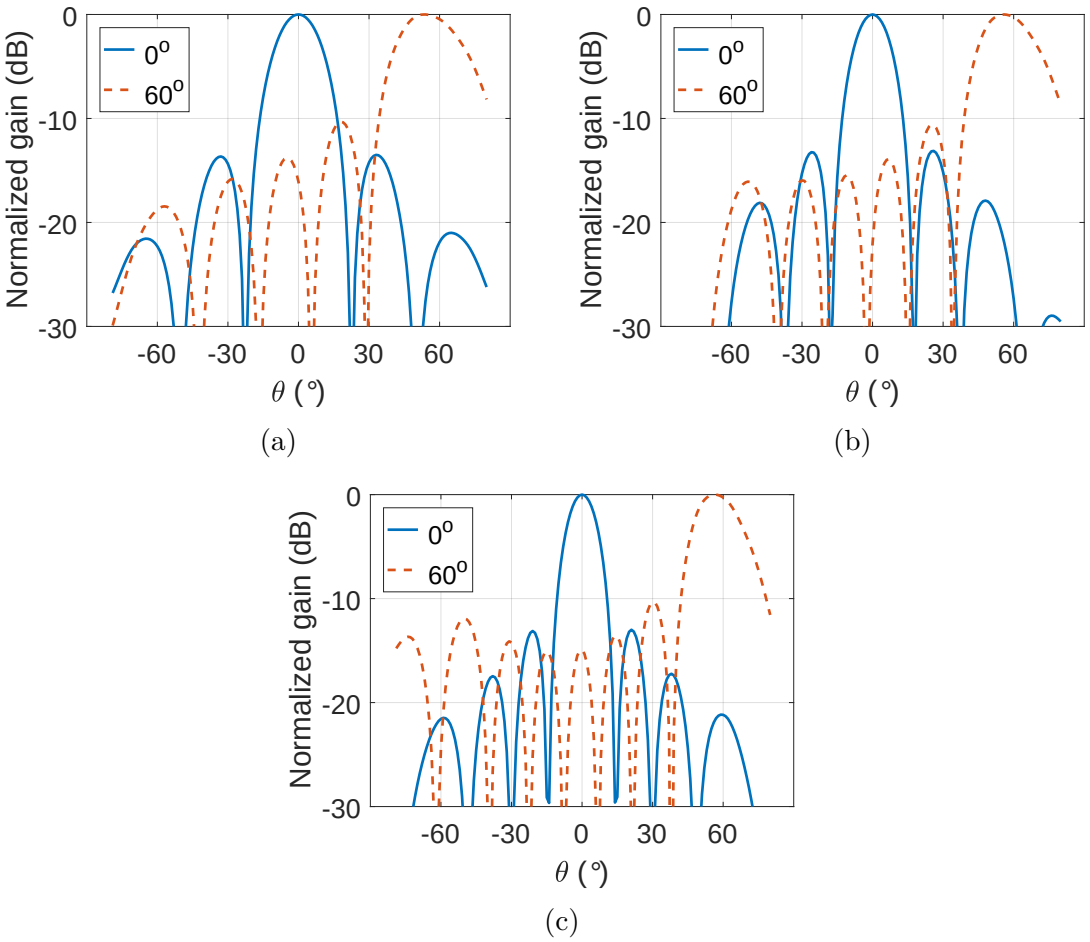

Figure 30: Normalized gain of an 8×8 array approximated from AEP when the array factor is steered to 0° and 60° on E-plane at (a) 26 GHz, (b) 33 GHz, and (c) 40 GHz.

4.4.3 Modified structure

The bent feed flared-notch antenna appears to be the most promising from all of the structures previously studied during this thesis when taking in the account the requirements, the performance, and the manufacturability. But even in this design, there might be some structures that would be hard to manufacture. For example, the small 0.2-mm diameter pin used to feed the slot line. The length of the pin in the previously simulated structure is 2.4 mm which might pose some problems as the diameter of the pin is very small and the pin might bend during the manufacturing. If the pin would be bent the impedance of the coaxial would change deteriorating the matching from the microstrip or stripline to the pin and from the pin to the slot line.

To decrease the length of the pin the element feed, the meandered slot line and the cavity had to be modified. The initial design and the modified design are shown in Figure 31. The width of the slot line is 0.4 mm and the thickness of the base plate

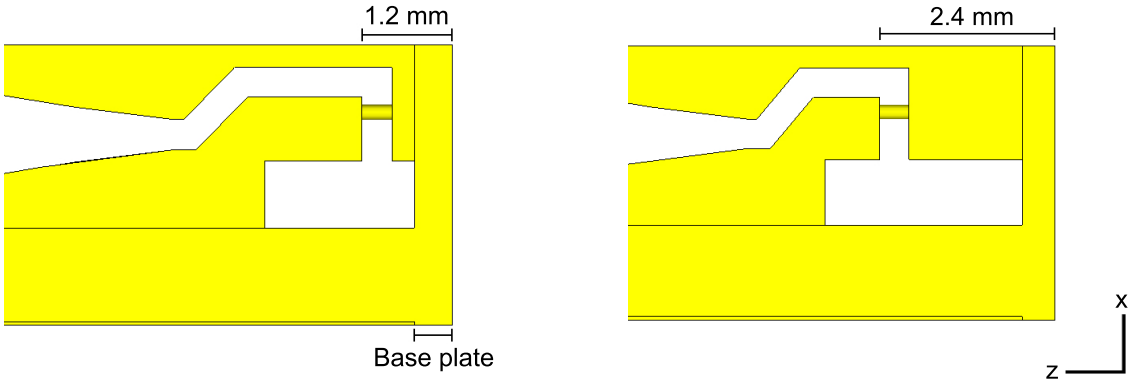

(a) (b)

Figure 31: In (a) the element with modified structure and shorter feed pin compared to the initial element in (b).

is 0.5 mm. This gives the absolute minimum length for the pin which is 0.9 mm. The slot line would in this case be situated next to the base plate and at the end of the cavity. As in the optimal case the slot line should be close to the center of the cavity so that the field in the cavity each side of the slot line would be similar. In a case where the slot line is in the other end of the cavity the field can not be similar and the matching will suffer. The optimal compromise, where the pin could be as short as possible and the matching would not suffer significantly is studied with simulations.

The optimally short length for the pin is determined to be 1.2 mm, a half of the initial value of 2.4 mm. The matching is optimized by decreasing the height of the cavity (along z-axis) from 2.7 mm to 2 mm. As the cavity still protrudes more above the slot line compared to the initial design, the length of the vertical part of the meandered slot line is increased by 0.6 mm. Additionally, the angle of the last part of the slot line before the exponential flare is decreased by 5°. The total length of

the element is decreased by 0.6 mm as a consequence. Rest of the design parameters are left as in the initial design.

The impact of the modifications is visible but not too significant that the design would be unusable. When comparing the active element impedance of the initial design in Figure 26 and the ARC of the modified element shown in Figure 32, most of the differences are located on the higher end of the band. While the ARC in the initial design was throughout the beam steering surface lower than −10 dB, in the modified design the ARC rises above −10 dB just before 39 GHz when steered to $\theta = \pm 60°$ on the E-plane ($\phi = 0°$). From 26 GHz to 38 GHz the ARC is lower than −10 in the whole beam steering surface.

The cross polarization of the modified structure is increased compared to the initial bent feed design and it is shown in Figure 33. That of the initial design, the maximum broadside cross polarization is increased from −17 dB to −14 dB and the minimum is increased from −23 dB to −18 dB. The minimum broadside cross polarization is observed on the lower end of the frequency range and the maximum is observed on the upper half of the frequency range. Overall, the cross polarization throughout the beam steering range is similar to the initial design but the level of the cross polarization is higher. The cross polarization is increased because the horizontal slot line is brought closer to the base plate and the fields close to the base plate are increased which in turn can add coupling to the other polarization. This is an unfortunate compromise which has to be made when the pin is made shorter. The maximum cross polarization is approximately −13.5 dB on the other diagonal plane ($\phi = -45°$). The coupling on the other diagonal plane ($\phi = 45°$) is a lot lower because of the asymmetric feed structure as in the initial design.

The total efficiency of the modified structure is shown in Figure 34. For the most parts, the efficiency stays above 90%. The overall efficiency is a couple percents lower than in the original design. The efficiency also drops after 38 GHz when steered on the E-plane to $\theta = 60°$ because of the ARC.

No major changes occur in the active element pattern and the pattern is free of any scan blindness as can be seen in Figure 35. Thus, the array gain of the 8×8 array shown in Figure 36 is also almost identical to the original design. Some minor changes can be observed at high angles because the AEP is slightly different but these changes are so small that they are irrelevant.

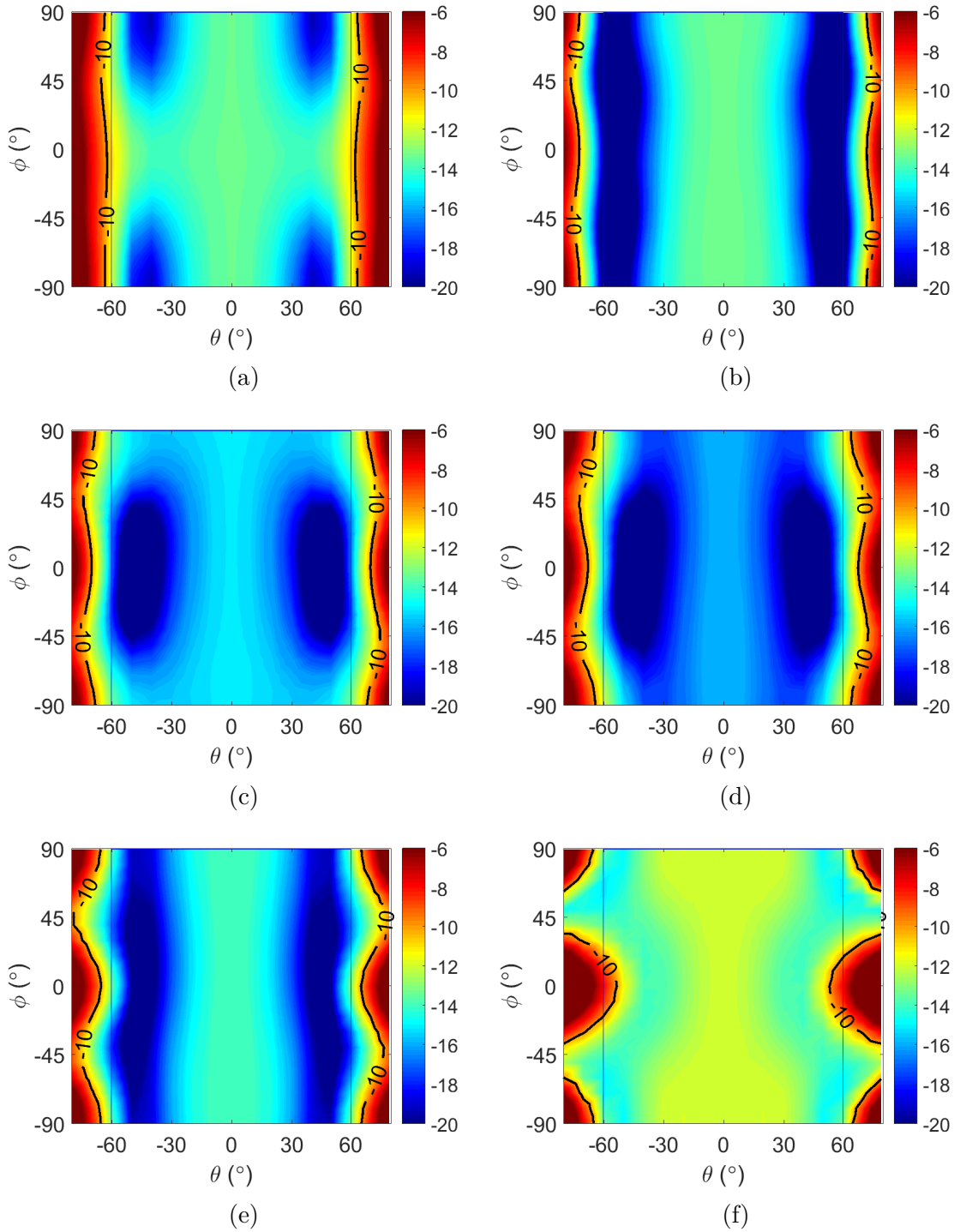

Figure 32: Active reflection coefficient of the modified bent feed flared-notch element infinite array on PCB at a) 26 GHz, b) 29 GHz, c) 32 GHz, d) 34 GHz, e) 37 GHz, and f) 40 GHz.

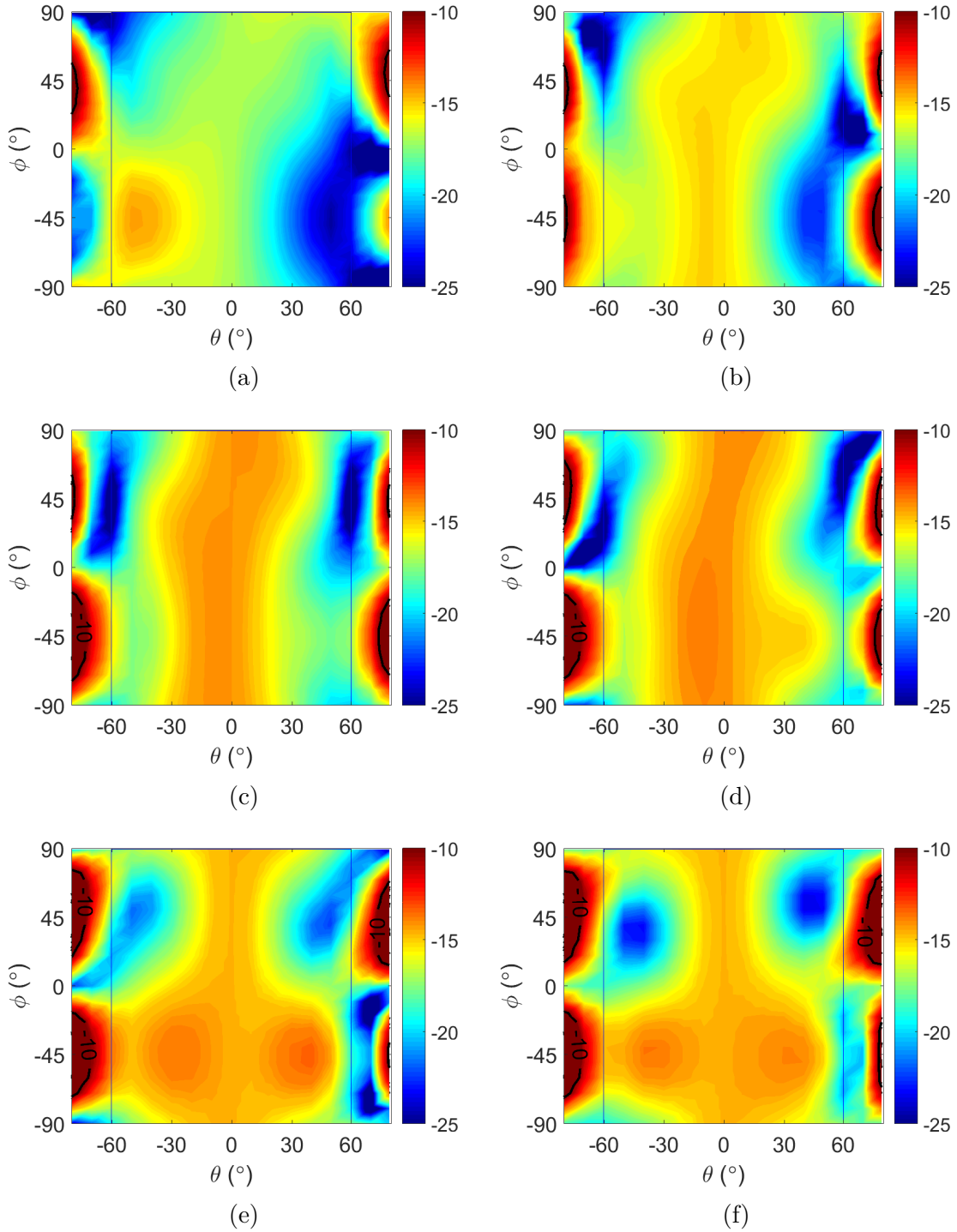

Figure 33: Cross polarization of the modified modified bent feed flared-notch element infinite array on PCB at a) 26 GHz, b) 29 GHz, c) 32 GHz, d) 34 GHz, e) 37 GHz, and f) 40 GHz.

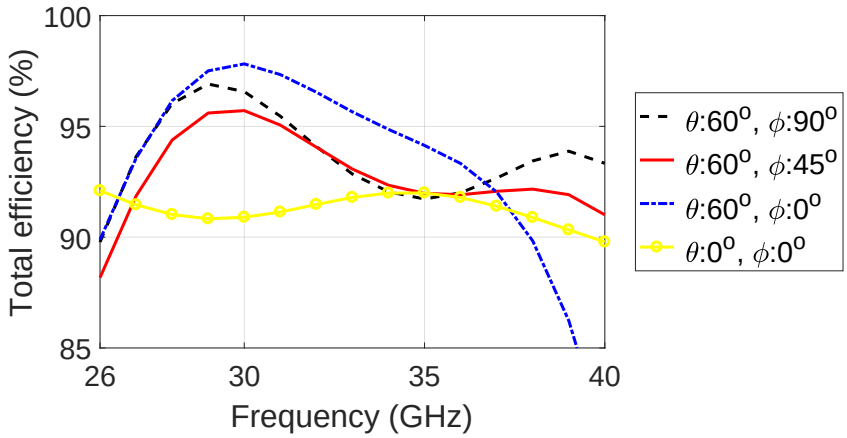

Figure 34: The efficiency of the modified bent feed flared-notch at different steering angles.

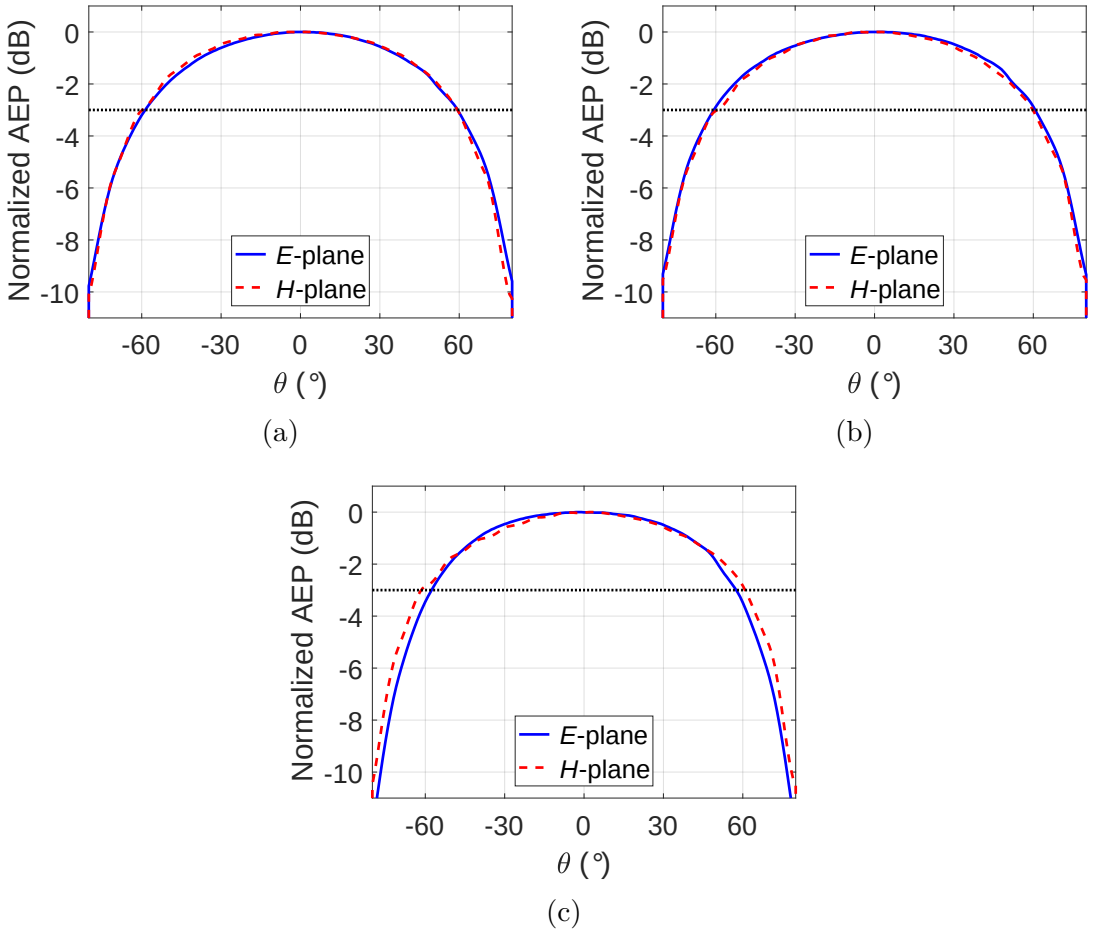

Figure 35: Normalized active element pattern of the the modified bent feed feed flared-notch in an infinite array on PCB at (a) 26 GHz, (b) 33 GHz, and (c) 40 GHz.

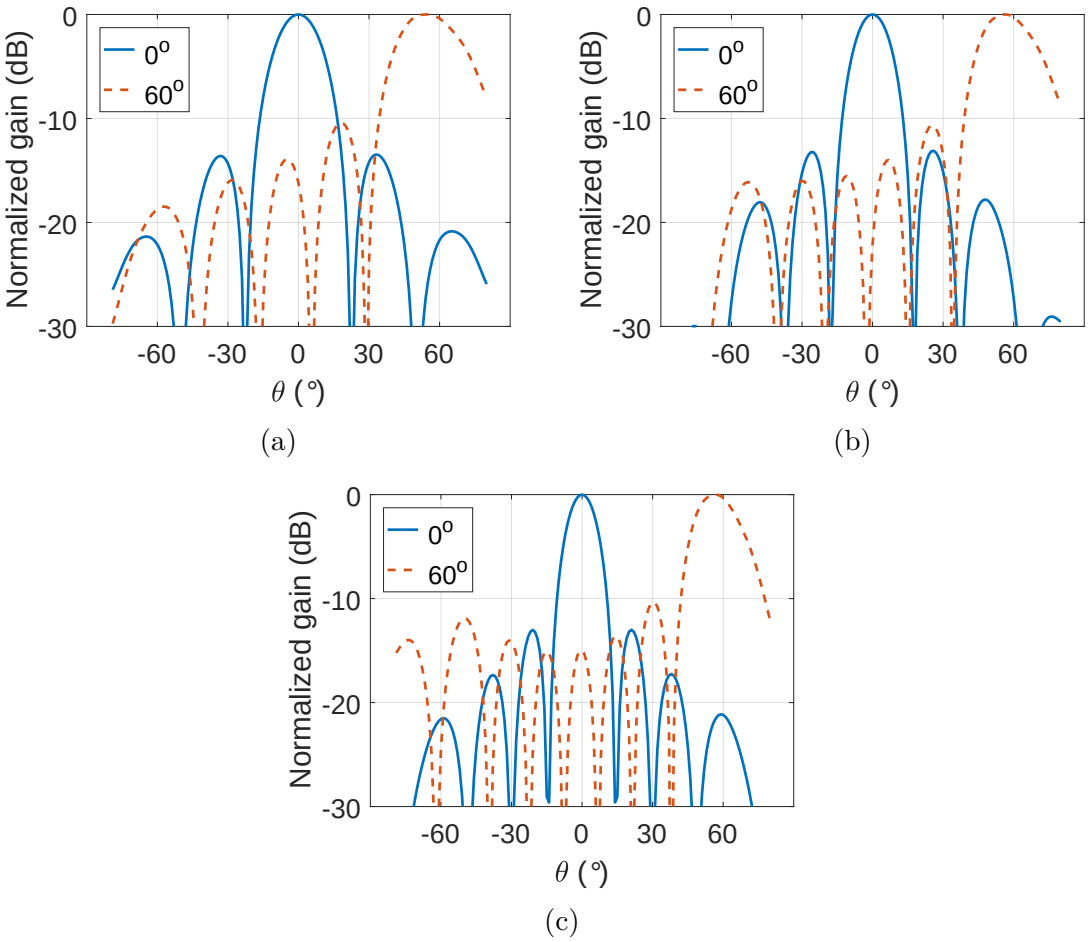

Figure 36: Normalized gain of an 8×8 array approximated from AEP when the array factor is steered to 0° and 60° on H-plane at (a) 26 GHz, (b) 33 GHz, and (c) 40 GHz.

5 Finite array simulations and comparison

The bent feed flared-notch element with shortened feed pin presented in section 4.4 is deemed to be the most suitable when the performance and manufacturing is taken into account. The antenna element is initially simulated and the performance was assessed in an infinite array. However, it is not possible to manufacture an infinite array but the performance of the array element can be assessed in a sufficiently large array as is explained in section 3.

There are no clear rules how large array is required to precisely approximate the characteristics of a middle element but the mutual coupling between two elements decreases as a function of the distance. It was decided that an 8×8 array should be sufficiently large as it is larger than one wavelength even at the lowest operation frequency.

It would be rather hard to try to measure the antenna under full excitation as each element would have to have a separate port. Optionally the elements could be fed with complex feeding network with power dividers but the properties of the single element could not be measured. The most feasible option would be to feed one middle element and terminate all other elements in matched load. This method can be used to measure the AEP of an element in the middle of the array which can be used as an approximate element pattern in a large array. The setup would not directly allow the measurement of the ARC but the reflection coefficients of the simulations and measurements from the middle element can be compared. The comparison of the simulated and measured reflection coefficient can then be used to conclude if the performance of the constructed and measured antenna is comparable to simulations and if the ARC of an infinite array would be a good approximation of a large array. The AEP measurements setup should also allow for a estimation of the level of cross polarization.

The effect of the array edges and the AEP of an element on the edge of the array can be studied by for example adding two additional feeds, one for an edge element and another for a corner element. This would not increase the complexity of the structure on the measurements, or the cost of a measurement prototype considerably.

The dual polarized 8×8 array constructed from the bent feed flared-notch elements and the simulation results are presented in this section.

5.1 Array structure

The array is constructed by grouping 64 dual polarized elements together and adding a small additional section of base plate around the array as is shown in Figure 37. Small additional part of the next unit cell is added to the last elements on the x- and y-axes to increase the mechanical strength of the prototype. This should not have any impact on the simulation results as the simulated elements are not on these edges. The same figure also shows the elements chosen to be excited. All the elements have the same x-oriented polarization and the fed elements are chosen so that one element is in the corner, two elements on the edges of the array, and one in the middle of the array. Two edge elements are chosen because the effect of

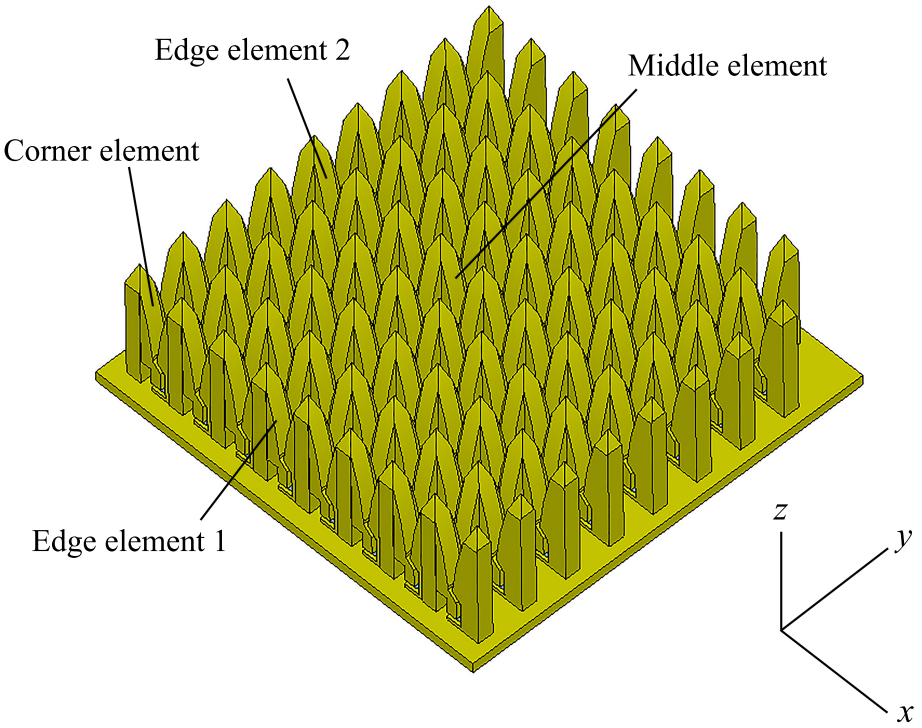

Figure 37: The simulated 8×8 array constructed from the bent feed flared-notch elements. The studied x-polarized elements are pointed

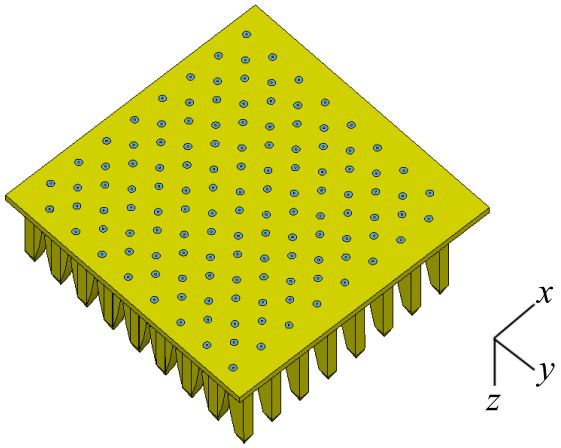

Figure 38: The bottom side of the simulated 8×8 array.

the edge is different depending on whether the polarization of the element is either perpendicular or parallel compared to the edge of the array.

The 128 feed ports for all 64 elements and both polarization can be seen on the bottom side of the structure in Figure 38. This structure itself can still only be used for simulations as there is no PCB to implement the microstrips and attach the connectors. The design of the PCB for the measurements is not within the scope of this thesis.

The reflection coefficient of each element in the manufactured structure including the microstrips and vias would be different and those have to be simulated separately before measurements. In this structure, the simulation result between the finite array and infinite array unit cell simulation can be more easily compared and the behavior of the antenna element can be observed.

5.2 Simulation results and comparison

Figure 39 shows the reflection coefficient of the middle element, the two edge elements, and the corner element. The result cannot be directly compared to the ARC but the matching of each element is roughly at the correct band. The frequency responses of the corner element and the edge element on the edge parallel to the polarization are quite similar but surprisingly the edge element on the edge perpendicular to the polarization has the lowest reflection coefficient. The reflection coefficient of the middle element is under −10 dB from 28 GHz to 42 GHz.

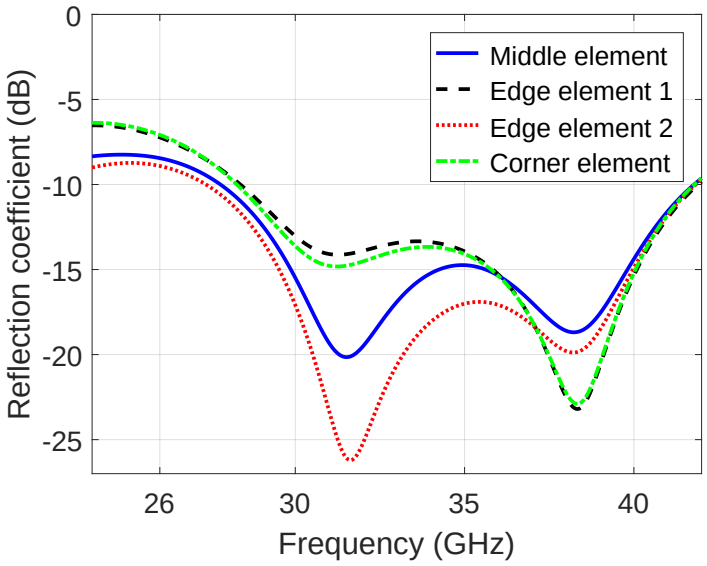

Figure 39: The reflection coefficients of middle, edge, and corner elements in an 8×8 array.

The comparison between the normalized simulated AEP (in infinite array) and the normalized gain of the middle array element in 8×8 array is shown in Figure 40 at 26, 33, and 40 GHz. At 33 and 40 GHz the pattern seems to behave quite nicely without taking into account the slight fluctuation caused by the finite number of elements in the array. At 26 GHz the 8×8 array might be too small especially on the H-plane. The E-plane pattern at 26 GHz is still performing quite satisfactorily. In all the other cases the HPBW is very close to the results simulated in an infinite array. The middle element in the 8×8 array is really not in the exact center of the array as the other side of the element has three and the other side four elements terminated in matched load. This can be especially seen in the E-field pattern at 26 GHz in which the gain drops below −3 dB at approximately 45°.

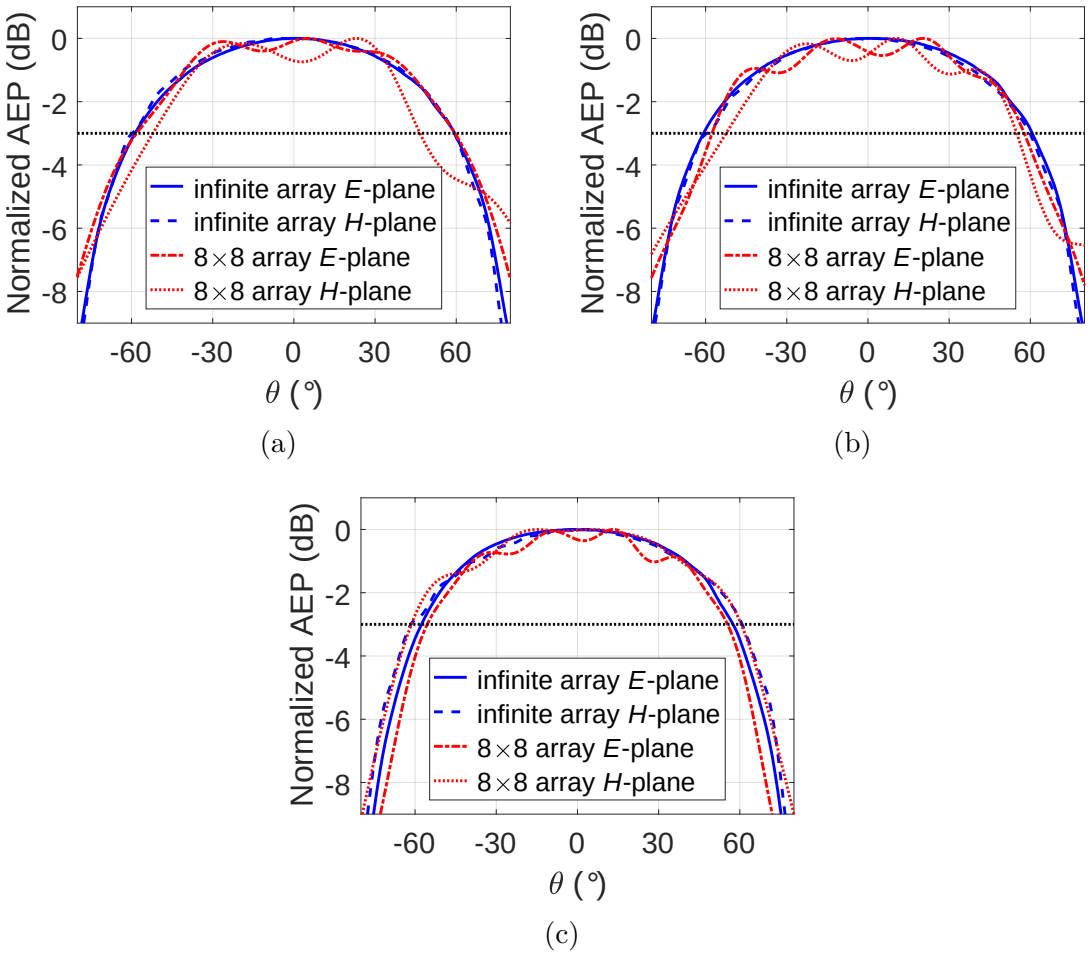

Figure 40: Comparison of the element pattern between the infinite array and middle element in the 8×8 array at (a) 26 GHz, (b) 33 GHz, and (c) 40 GHz.

The radiation pattern of the edge and the corner elements at 26, 33, and 40 GHz are shown in Figure 41. Each of the pattern in these figures is normalized with respect to the middle element to emphasize the change in the gain. In all cases, the broadside gain of the elements at the edge of the array is 0.5–2.5 dB lower than the broadside gain of the middle element. The effect of the edge is most visible in the patterns which are perpendicular to the edge of the array, i.e., in corner element patterns in both the E- and the H-planes, for the edge element 1 pattern in the H-plane, and for the edge element 2 pattern in the E-plane. The radiation pattern is most distorted on these planes at steering angles away from the array ($\theta < 0°$). The radiation pattern of the element in the corner is affected the most and the edge element 2 is affected the least. The pattern of the edge element 2 performs well compared to the edge element 1 when the difference between the elements is that the edge element 1 is on a edge parallel to the polarization and edge element 2 is on a edge perpendicular to the polarization. The behavior in the patterns

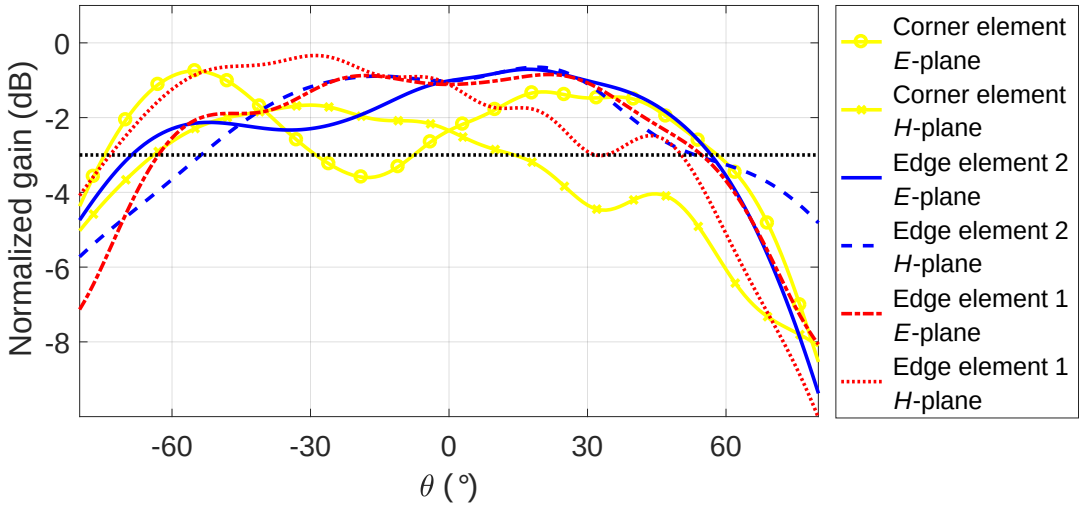

(a)

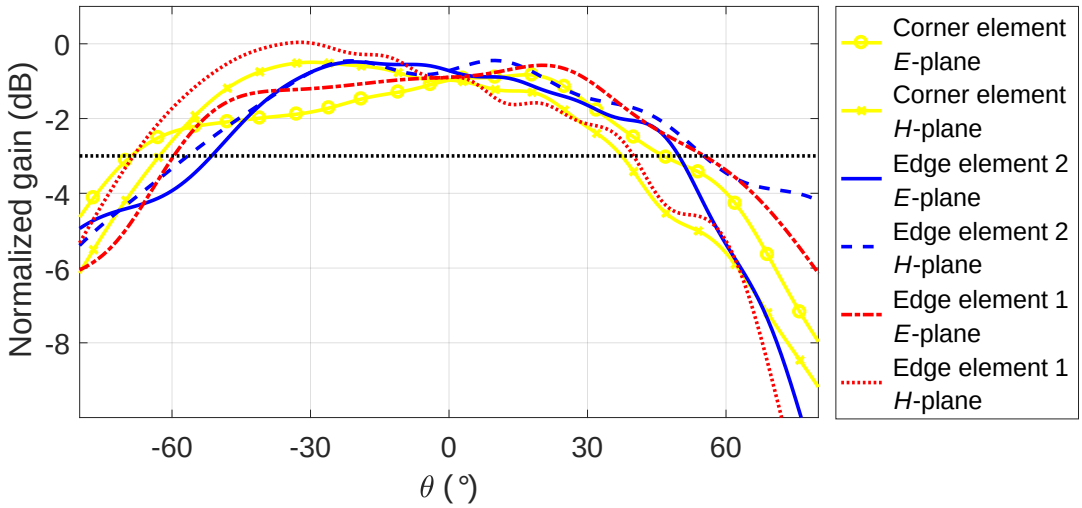

(b)

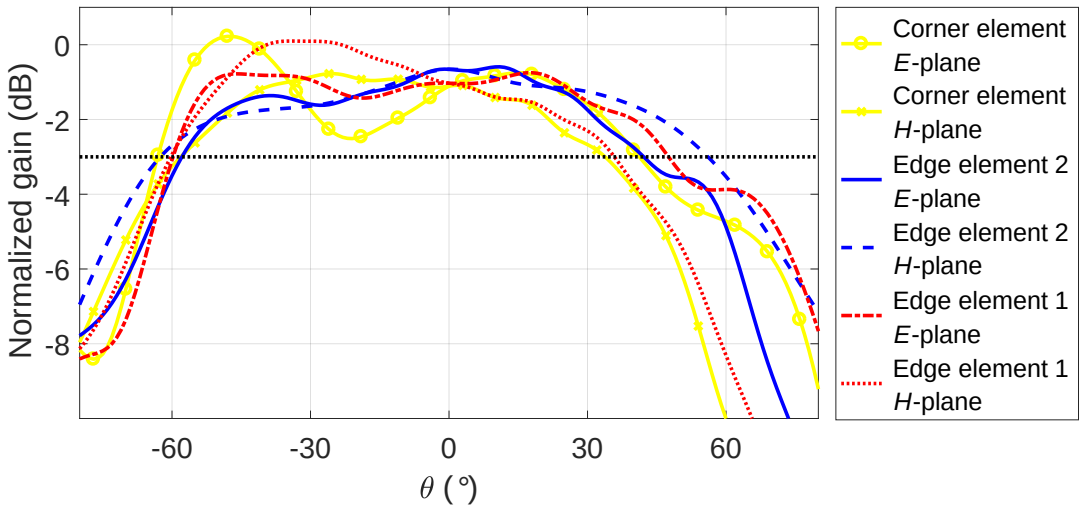

(c)

Figure 41: The gain of the edge elements and the corner element at (a) 26 GHz, (b) 33 GHz, and (c) 40 GHz normalized with respect to the middle element.

6 Conclusions

The purpose of the work in this thesis was to study possible antenna structures for Ka-band phased array and validate the performance of promising structures with simulations. A literature survey covering antenna elements suitable for phased arrays and previous research on phased arrays was carried out. The stacked patch antenna and flared-notch antenna were selected to be studied with simulations. In addition, optimized bent feed flared-notch antenna element was then simulated in the 8×8 array so that it could later be manufactured and measured to assess the manufacturability and the performance.

Single polarized aperture coupled stacked patch array is relatively simple planar structure which could be manufactured with similar processes as PCBs. The element size of one element at this frequency is already quite small which makes it challenging to design a dual polarized feed for aperture coupled patches. However, previous studies have shown that this kind of feeds are possible and with further study it should be possible to implement dual polarized feed for this element. The performance of the studied element did not meet the performance requirements throughout the whole frequency band partially due to the scan blindness at higher frequencies.

The flared-notch structures demonstrate better performance figures than the aperture coupled stacked patch. Additionally, the implementation of dual polarized feed into the flared notch structure is more simple. Two different flared-notch elements were studied due to the expected challenges in the manufacturing the first design. The design that is chosen for the 8×8 array simulations is the bent feed flared-notch element with the shorter feed pin. The performance of the final structure in unit cell simulations is very close to meeting the proposed performance figures. Only exception being the slight dip in performance on E-plane when the beam is scanned to 50° or more above 38 GHz. On E-plane at 40 GHz the efficiency of the antenna drops at worst to 80% due to ARC increasing over −10 dB. The ARC is lower than −10 dB throughout the frequency band and scan angles except at the aforementioned case on E-plane. The AEP of the element can be said to be frequency independent as it is almost constant as a function of frequency. The HPBW of the element pattern at all frequencies is approximately 120°.

The performance of the bent feed flared-notch element in the finite array is well in line with the results simulated previously in infinite array unit cell simulations. At the higher part of the array bandwidth the element pattern of the middle element is very similar to the element pattern in infinite array. Only at the lower end of the frequency band the 8×8 array is electrically too small as the element pattern in finite array at 26 GHz fluctuates significantly.

The 8×8 array that has been design and simulated during this thesis is manufacturable with additive manufacturing or wire EDM. The structure will be prepared for manufacturing in a following project. The design of the PCB used for feeding the elements will also be designed during the continuation project as it was not in the scope of this thesis.

References

[1] I. S. Merrill *et al.*, *Introduction to radar systems*. Mc Grow-Hill, 2001.

[2] D. C. Schleher, "Introduction to electronic warfare," Eaton Corp., AIL Div., Deer Park, NY, Tech. Rep., 1986.

[3] R. J. Mailloux, *Phased array antenna handbook*. Artech House Boston, 2005, vol. 2.

[4] Saab AB, Stockholm, Sweden, [Online]. Available: http://www.saabgroup.com.

[5] "IEEE standard for definitions of terms for antennas," *IEEE Std 145-2013 (Revision of IEEE Std 145-1993)*, pp. 1–50, March 2014.

[6] A. S. Committee *et al.*, "IEEE standard test procedures for antennas," *ANSI/IEEE Std 149-1979*, pp. 1949–1979, 1979.

[7] W. L. Stutzman and G. A. Thiele, *Antenna Theory and Design*. John Wiley & Sons, 2012.

[8] C. A. Balanis, *Antenna theory: analysis and design (3rd ed.)*. John Wiley & Sons, 2005.

[9] J. Dyson, "The equiangular spiral antenna," *IRE Transactions on Antennas and Propagation*, vol. 7, no. 2, pp. 181–187, April 1959.

[10] R. DuHamel and D. Isbell, "Broadband logarithmically periodic antenna structures," in *1958 IRE International Convention Record*, vol. 5, March 1957, pp. 119–128.

[11] P. J. Gibson, "The Vivaldi aerial," in *1979 9th European Microwave Conference*, Sept. 1979, pp. 101–105.

[12] J. Jung, W. Choi, and J. Choi, "A small wideband microstrip-fed monopole antenna," *IEEE Microwave and Wireless Components Letters*, vol. 15, no. 10, pp. 703–705, Oct. 2005.

[13] J. Kim, C. S. Cho, and J. W. Lee, "5.2 GHz notched ultra-wideband antenna using slot-type SRR," *Electronics Letters*, vol. 42, no. 6, pp. 315–316, March 2006.

[14] F. Croq and A. Papiernik, "Large bandwidth aperture-coupled microstrip antenna," *Electronics Letters*, vol. 26, no. 16, pp. 1293–1294, Aug 1990.

[15] S. D. Targonski, R. B. Waterhouse, and D. M. Pozar, "Wideband aperture coupled stacked patch antenna using thick substrates," *Electronics Letters*, vol. 32, no. 21, pp. 1941–1942, Oct. 1996.

[16] ——, "Design of wide-band aperture-stacked patch microstrip antennas," *IEEE Transactions on Antennas and Propagation*, vol. 46, no. 9, pp. 1245–1251, Sep 1998.

[17] A. A. Serra, P. Nepa, G. Manara, G. Tribellini, and S. Cioci, "A wide-band dual-polarized stacked patch antenna," *IEEE Antennas and Wireless Propagation Letters*, vol. 6, pp. 141–143, April 2007.

[18] J. Shin and D. H. Schaubert, "A parameter study of stripline-fed Vivaldi notch-antenna arrays," *IEEE Transactions on Antennas and Propagation*, vol. 47, no. 5, pp. 879–886, May 1999.

[19] K. S. Yngvesson, T. Korzeniowski, Y.-S. Kim, E. L. Kollberg, and J. F. Johansson, "The tapered slot antenna-a new integrated element for millimeter-wave applications," *IEEE Transactions on Microwave Theory and Techniques*, vol. 37, no. 2, pp. 365–374, 1989.

[20] D. Schaubert, S. Kasturi, A. Boryssenko, and W. Elsallal, "Vivaldi antenna arrays for wide bandwidth and electronic scanning," in *Antennas and Propagation, 2007. EuCAP 2007. The Second European Conference on.* IET, 2007, pp. 1–6.

[21] S. Livingston and J. Lee, "A low profile wide band dual-pol array with coincident phase center for next generation radars," in *Radar Systems (Radar 2012), IET International Conference on.* IET, Oct. 2012, pp. 1–5.

[22] R. C. Hansen, *Phased Array Antennas.* John Wiley & Sons, 2009, vol. 213.

[23] P. Hannan and M. Balfour, "Simulation of a phased-array antenna in waveguide," *IEEE transactions on Antennas and Propagation*, vol. 13, no. 3, pp. 342–353, 1965.

[24] D. M. Pozar, "A relation between the active input impedance and the active element pattern of a phased array," *IEEE Transactions on Antennas and Propagation*, vol. 51, no. 9, pp. 2486–2489, Sept. 2003.

[25] ——, "The active element pattern," *IEEE Transactions on Antennas and Propagation*, vol. 42, no. 8, pp. 1176–1178, Aug. 1994.

[26] CST Computer Simulation Technology AG, Darmstadt, Germany. "CST MICROWAVESTUDIO®", [Online]. Available: https://www.cst.com/products/cstmws.

[27] M. Rütschlin, T. Wittig, and Z. Iluz, "Phased antenna array design with CST STUDIO SUITE," in *2016 10th European Conference on Antennas and Propagation (EuCAP)*, April 2016, pp. 1–5.

[28] H. Holter, "Dual-polarized broadband array antenna with BOR-elements, mechanical design and measurements," *IEEE Transactions on Antennas and Propagation*, vol. 55, no. 2, pp. 305–312, Feb 2007.

[29] ——, "A new type of antenna element for wide-band wide-angle dual polarized phased array antennas," in *IEEE International Symposium on Phased Array Systems and Technology, 2003.*, Oct. 2003, pp. 393–398.

[30] R. W. Kindt and W. R. Pickles, "Ultrawideband all-metal flared-notch array radiator," *IEEE Transactions on Antennas and Propagation*, vol. 58, no. 11, pp. 3568–3575, Nov 2010.

[31] S. B. Cohn, "Slot line on a dielectric substrate," *IEEE Transactions on Microwave Theory and Techniques*, vol. 17, no. 10, pp. 768–778, Oct. 1969.

[32] D. M. Pozar, *Microwave Engineering (4th ed.).* Hoboken, NJ: Wiley, 2012.